

SANDIA REPORT

SAND97-8278 • UC-408

Unlimited Release

Printed August 1997

Miniature Gamma-Ray Camera for Tumor Localization

J. C. Lund, R. W. Olsen, R. B. James, E. Cross, H. Hermon, D. S. McGregor,
N. R. Hilton, J. E. McKisson, J. M. Van Scyoc, H. Yoon, B. A. Brunett,
W. W. Moses, E. Beauville, J. G. Kelley, F. P. Doty, B. E. Patt, D. Wolfe

Prepared by

Sandia National Laboratories

Albuquerque, New Mexico 87185 and Livermore, California 94550

Sandia is a multiprogram laboratory operated by Sandia Corporation,
a Lockheed Martin Company, for the United States Department of
Energy under Contract DE-AC04-94AL85000.

Approved for public release; distribution is unlimited.



Sandia National Laboratories

Issued by Sandia National Laboratories, operated for the United States Department of Energy by Sandia Corporation.

NOTICE: This report was prepared as an account of work sponsored by an agency of the United States Government. Neither the United States Government nor any agency thereof, nor any of their employees, nor any of their contractors, subcontractors, or their employees, makes any warranty, express or implied, or assumes any legal liability or responsibility for the accuracy, completeness, or usefulness of any information, apparatus, product, or process disclosed, or represents that its use would not infringe privately owned rights. Reference herein to any specific commercial product, process, or service by trade name, trademark, manufacturer, or otherwise, does not necessarily constitute or imply its endorsement, recommendation, or favoring by the United States Government, any agency thereof, or any of their contractors or subcontractors. The views and opinions expressed herein do not necessarily state or reflect those of the United States Government, any agency thereof, or any of their contractors.

Printed in the United States of America. This report has been reproduced directly from the best available copy.

Available to DOE and DOE contractors from
Office of Scientific and Technical Information
P.O. Box 62
Oak Ridge, TN 37831

Prices available from (615) 576-8401, FTS 626-8401

Available to the public from
National Technical Information Service
U.S. Department of Commerce
5285 Port Royal Rd
Springfield, VA 22161

NTIS price codes
Printed copy: A04
Microfiche copy: A01

Miniature Gamma-Ray Camera for Tumor Localization

J. C. Lund, R. W. Olsen, R. B. James, E. Cross, H. Hermon, D. S. McGregor
Sandia National Laboratories, P. O. Box 969, Livermore, CA 94551

N. R. Hilton
University of Arizona, Tucson, AZ 85724

J. E. McKisson
Radiation Technologies, Inc., Alachua, FL 32615

J. M. Van Scyoc, H. Yoon
University of California, Los Angeles, CA 90024

B. A. Brunett
Carnegie Mellon University, Pittsburgh, PA 15213

W. W. Moses, E. Beauville
Lawrence Berkeley Laboratory, Berkeley, CA 94720

J. G. Kelley
Sandia National Laboratories, P. O. Box 5800, Albuquerque, NM 87185

F. P. Doty
Digirad, San Diego, CA 92121

B. E. Patt
Xsirius, Inc., Camarillo, CA 93012

D. Wolfe
University of New Mexico, Albuquerque, NM 87185

ABSTRACT

The overall goal of this LDRD project was to develop technology for a miniature gamma-ray camera for use in nuclear medicine. The camera will meet a need of the medical community for an improved means to image radio-pharmaceuticals in the body. In addition, this technology-with only slight modifications- should prove useful in applications requiring the monitoring and verification of special nuclear materials (SNMs). Utilization of the good energy resolution of mercuric iodide and cadmium zinc telluride detectors provides a means for rejecting scattered gamma-rays and improving the isotopic selectivity in gamma-ray images. The first year of this project involved fabrication and testing of a monolithic mercuric iodide and cadmium zinc telluride detector arrays and appropriate collimators/apertures. The second year of the program involved integration of the front-end detector module, pulse processing electronics, computer, software, and display.

ACKNOWLEDGMENT

We gratefully acknowledge support of this project by Laboratory Directed Research and Development (LDRD) funds (case #3514.090). In addition we would like to acknowledge the efforts of the various graduate students and researchers who have contributed to this effort and have helped to make this project a success.

CONTENTS

| | |
|--|----|
| Preface | 6 |
| Summary | 7 |
| Nomenclature | 8 |
| Introduction | 9 |
| Background | 9 |
| System Design | 10 |
| Detector Design and Fabrication | 12 |
| Electronic Readout | 12 |
| Software | 20 |
| System Testing | 20 |
| Uniformity of Semiconductor Materials | 24 |
| Conclusions | 27 |
| References | 28 |
| APPENDIX A - Publications Resulting from this Work | 29 |

PREFACE

The ability to simultaneously image and perform spectroscopy on gamma ray photons is important in a number of fields. In Nuclear Medicine, gamma ray imaging is used to locate the presence of radiopharmaceuticals in the patient's body, and the spectroscopic information is used to reduce background and reject scattered gamma rays. In the areas of Environmental Monitoring and SNM inspection, it is necessary to both locate the presence of radioactive materials (through imaging) and identify the type of radioisotope causing the emission (through spectroscopy of the gamma-ray emissions). The conventional technology for performing gamma-ray imaging to date has been the Anger Gamma-Camera. An Anger camera consists of one more slabs of an inorganic scintillator (usually NaI(Tl)) to which are attached a number of photomultiplier tubes (PMTs). The very large size of the PMT/scintillator in a conventional gamma camera is useful in some applications (such as whole body imaging or counting), but the large size of these devices prevents their use in many applications such as intra-operative medical use or remote in-situ monitoring of SNMs. Another flaw in conventional gamma cameras is their poor energy resolution when operated as a spectrometer. Anger cameras are inherently limited by the statistics of scintillator photon production to energy resolutions of about 10% FWHM at moderate photon energies (500 keV to 1 MeV) and worse resolutions at lower energies (the resolution goes as $E^{-1/2}$). The relatively poor energy resolution of scintillator-based instruments limits their utility in applications- such as isotope identification- that require the discrimination of closely spaced peaks in the gamma-ray pulse height spectrum.

The emergence of room-temperature semiconductor detector crystals such as HgI_2 and $\text{Cd}_{(1-x)}\text{Zn}_x\text{Te}$ (CZT) has opened up the possibility of a new type of gamma-ray imaging detector based on monolithic arrays of detectors. If suitable arrays of detectors could be made from these materials (and suitable electronics could be built to read them out), then semiconductor arrays could replace conventional Anger cameras in many applications well as open up a wide variety of new applications. Semiconductor arrays of CZT or HgI_2 should be capable of much better position resolution at the image plane than PMT-based cameras owing to the very small sizes in which the semiconductor pixels can be made. Furthermore, the energy resolution of semiconductor-based systems is much better than scintillator systems - particularly at lower photon energies (<200 keV) - owing to the more favorable statistics of electron-hole pair production in these semiconductor materials.

However, significant technical problems exist with these new semiconductor materials, and a variety of technologies must be developed to solve the problems associated with building gamma-cameras from room-temperature semiconductor materials. In particular, methods must be developed to design and fabricate suitable detector arrays from these materials and methods must be developed for reading out the very large number of anticipated pixels (>1000) with portable electronics at reasonable cost per channel. The primary objective of the project described in this report was to solve these problems, and substantial progress was made in this direction.

SUMMARY

The objective of this project was to improve the technology used with semiconductor - based gamma-cameras to the point where these gamma cameras would be useful in applications. We met this objective by developing new technological capabilities in two areas: the design and construction of pixellated semiconductor detector arrays, and the development of readout electronics and software capable of producing an image from these new devices. In particular, orthogonal strip detectors were fabricated from both HgI_2 and CZT during the course of this investigation. Electronics, based first on hybrid technologies, and later on application specific integrated circuits, was also developed in conjunction with software that allowed the simultaneous encoding of position and energy resolution from gamma-rays that interacted with these new devices. Thus the work that was performed within the framework of this project led to the development of improved methods for producing and reading out semiconductor gamma-ray detector arrays. We can unequivocally state that all the milestones established for this program were met or exceeded.

NOMENCLATURE

| | |
|------------------|---|
| ADC | analog to digital converter |
| ASIC | application specific integrated circuit |
| CAMAC | a computer interfacing standard for nuclear electronics |
| CMOS | complimentary metal oxide semiconductor |
| CZT | cadmium zinc telluride |
| DIP | dual inline package |
| GUI | graphical user interface |
| HgI ₂ | mercuric iodide |
| NIM | nuclear instrumentation module |
| PMT | photomultiplier tube |
| SNM | special nuclear material |
| Z | atomic mass |

Miniature Gamma-Ray Camera for Tumor Localization

Introduction

Gamma-ray spectrometers made from wide band-gap materials (such as mercuric iodide, cadmium telluride, and- more recently- cadmium zinc telluride) have been under development for many years. Substantial improvements have been made during this time period in the development of the quality of crystals available from these materials and methods to utilize them as detectors for gamma-rays. In the last decade attempts have been made to construct not only gamma-ray spectrometers from wide band-gap materials but spectrometers capable of encoding the position of interaction of the gamma-ray on the detector plane. Position sensitive detector arrays, coupled with an appropriate collimator, comprise a complete gamma-ray imaging system or "gamma camera". The possibility of constructing gamma-cameras from semiconductor materials is very enticing, as semiconductor detectors offer many advantages over the scintillator/PMT technology used in conventional gamma cameras. Both the energy resolution and position resolution on the detector plane should be much better for a semiconductor versus an Anger camera based on scintillator/PMT technology. Despite the potential promise of semiconductor gamma cameras, significant technical problems must be overcome before these devices can be widely deployed. During the project on which this report is based, substantial progress was made in solving many of these technical difficulties, but some difficulties remain. Before we discuss the technical details of the gamma camera development project, it is first useful to review the technical background that enables the operation of these devices, and to review the technical advantages that semiconductor detectors have in this application.

Background

Gamma cameras have been in wide use in nuclear medicine for many years and currently represent a commercial annual market of several billion US dollars. The conventional gamma camera employed in a hospital today consists of an Anger camera; a device consisting of an array of PMTs attached to a large (approximately 1.0 meter in diameter) crystal of inorganic scintillating material such as NaI(Tl) or BGO. When a gamma-ray photon interacts with the scintillating crystal in a gamma-camera, it produces an energetic electron via a photo-electric or Compton scattering process. The energetic electron produced by gamma ray interaction subsequently deposits its energy within a millimeter or so of the gamma-ray interaction site. When the electron loses its energy it produces scintillating photons which are detectable by the PMTs. By determining the position centroid (Anger logic) of the light detected from several PMTs, the position of interaction of the photon can be determined. The scintillators used in conventional gamma cameras require some tens of eV of energy deposited to produce a single scintillating photon. Thus only a few tens of optical photons are produced per keV of gamma ray detected. This low number of photons- or more accurately the statistical fluctuation in this number of photons- ultimately determines both the energy and position resolution of the detector used in existing gamma camera systems. The resolution with which a gamma-camera can encode position on the detector is not the same as the spatial resolution with which the gamma camera system can estimate gamma emission in a patient. The position resolution of the collimator is also an important factor; in general, the position resolution in the resultant

image is the convolution of the spatial response function of the collimator and the spatial response function of the detector. In modern large gamma cameras, the position resolution of the system is usually determined by the collimator. However, in a portable system employing a high resolution collimator (such as a pinhole collimator), the system resolution would be determined by the position resolution of the detector plane. Under these circumstances (i.e. portable gamma-cameras) the position resolution of the gamma ray imager is limited by the scintillator /PMT detector. Furthermore, if one seeks to determine the isotope that produces the gamma ray emission, the ability to resolve isotopes is severely limited by the energy resolution of the scintillator-based detector system.

An obvious method for overcoming the limitations of scintillator-based systems is to use a semiconductor-based system. In a semiconductor detector, only a few eV are required to produce an electron-hole pair. Furthermore, the generation of the charge pairs is a sub-Poissonian process (fluctuation is less than a random process), resulting in much better energy resolution and potentially better position resolution as well. Indeed, semiconductor gamma ray spectrometers made from germanium long ago displaced scintillation systems as the best detection technique for energy spectroscopy. However, because of the cryogenic cooling involved, it is not practical to use a conventional germanium detector in this application. Instead, the obvious solution to producing improved miniature gamma-cameras is to use room temperature semiconductor materials (such as HgI₂ and CZT) to build the detectors. Thus, the central goal of the project described in this report was to define the critical technologies that are impeding the development of position sensitive detectors. The details of this investigation are described in the subsequent sections of this report.

System Design

There are several approaches that might be tried to produce a semiconductor detector with imaging capabilities. The most obvious solution is to configure a square array of individual detector elements into the desired image plane. However, since a typical imager useful in medical situations would require at least a square array of dimensions 32 x 32 elements (1024 total elements), it is not economical to fabricate and assemble into an array such a large number of individual elements.

The next most obvious approach is to fabricate a monolithic array of individual detector elements on a single semiconductor substrate. If lithographic approaches to fabrication are used, it becomes practical to fabricate monolithic arrays with a suitable number of elements. However, reading out the signal from such an array would require very complex electronics. In general, to readout an N x N array of individual pixels requires N² separate channels of readout electronics; for arrays larger than about 4x4 this becomes a very complex solution, particularly since each channel of electronics must be very high performance (low noise) to take advantage of the benefits of semiconductor detectors.

An alternative approach to reading out a semiconductor detector array was first proposed by Gerber et al is known as an orthogonal strip design. Such an approach is illustrated in Figure 1 and consists of rows of parallel electrical contacts (strips) placed at right angles to each other on opposite sides of the detector. By making use of the temporal coincidence between events on both sides of the detector, it is possible to readout an array of N² effective detector elements using only 2N channels of readout electronics. We decided to utilize the orthogonal strip approach for all of the detectors we designed and built in the course of this program.

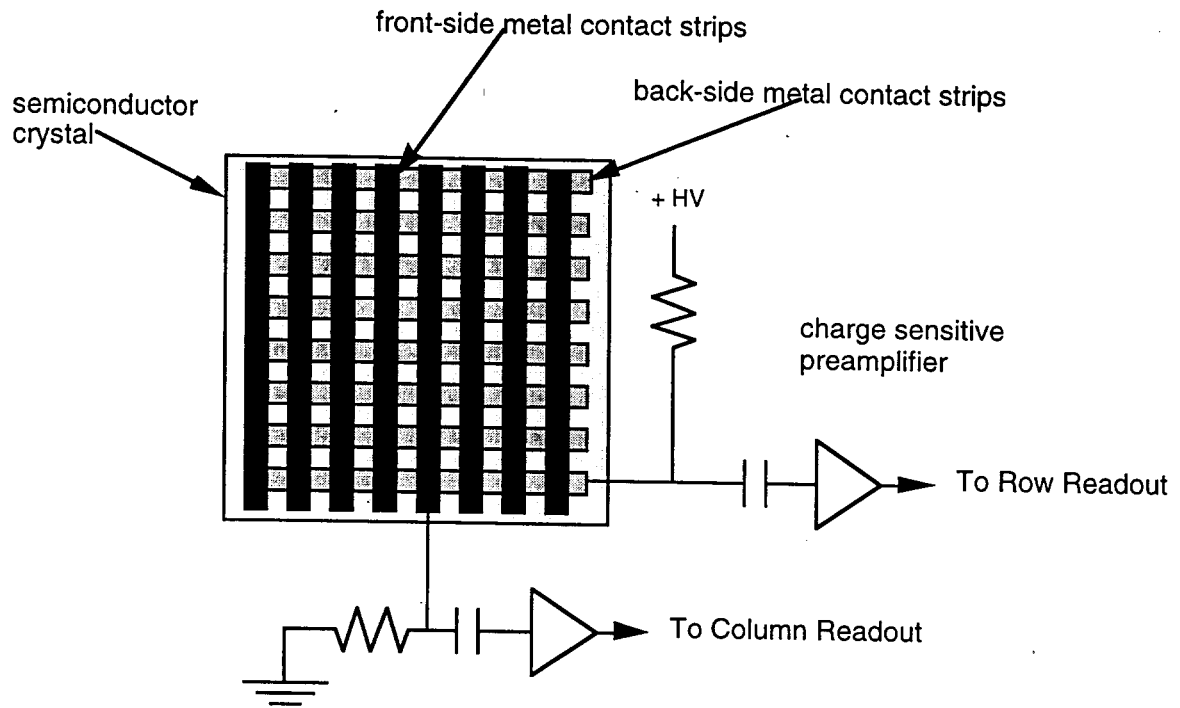


Figure 1. Diagrammatic view of an “8x8” orthogonal strip detector and front-end readout electronics. The metal contact strips are deposited on opposite sides of a square piece of semiconductor wafer. Event localization on the detector plane is determined by scoring a coincidence event between a column and a row. Using this method reduces the complexity of the readout electronics considerably. In general, to readout an array of N^2 effective pixels only requires $2 \times N$ channels of readout electronics, as opposed to N^2 channels of readout required for a detector consisting of an array of individual pixels.

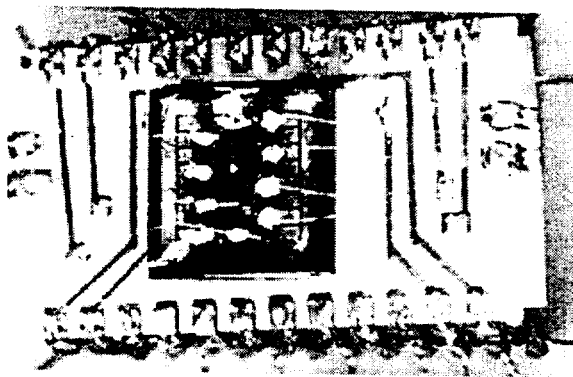


Figure 2. Photograph of an 8x8 orthogonal strip CZT detector mounted on a ceramic 24 pin DIP package.

Detector Design and Fabrication

Detectors were designed and built using both HgI_2 and CZT materials as substrates. Our first detectors were 8x8 devices fabricated on HgI_2 and CZT substrates approximately 2mm thick. These 8x8 orthogonal strip detectors resulted in devices with 64 effective pixels with each pixel a square of approximately $0.125 \times 0.125 \text{ cm}^2$ dimensions. These devices were placed on chip carriers (see Figure 2) that allowed them to be plugged directly into the readout electronics which was undergoing parallel development.

Detectors were fabricated by evaporating metal contacts on to the surface of etched crystal substrates using a shadow mask to define the strip pattern. Later in the project high density 16x16, 32x32, and 64x64 strip devices were fabricated using photolithographic techniques. Lithographic techniques were used on the high pixel density devices because the shadow mask technology would not provide adequate resolution. These high density devices were fabricated on CZT substrates alone because suitable lithographic methods do not exist for applying contacts to mercuric iodide detectors.

The photomask design used to create the high density 32x32 and 64x64 devices is shown in Figure 3. Figure 4 shows some photographs of the completed high density CZT imaging arrays.

During the course of our investigation, we became aware of two other groups^{1,2} that began performing research very similar to ours in the area of gamma-ray imaging. These groups were developing orthogonal strip CZT detectors for astronomical applications (gamma -ray telescopes). Subsequent discussions and collaboration with these groups were helpful, particularly in eliminating less promising research directions.

Electronic Readout

As mentioned in the previous sections, a significant problem in building a gamma camera from semiconductor materials is the design of the electronics system that is used to readout the detector. A very large number of pixels must be read, and good pulse height energy resolution must be attained for each individual pixel. Two types of electronic readout system were developed in the course of the research program described in this report. The first system- used to readout the 8x8 detector arrays- made use of hybrid preamplifiers followed by NIM and CAMAC readout amplifiers and ADCs. Later in the program an ASIC was developed (in collaboration with Lawrence Berkeley National Laboratory) to provide a larger number of channels for readout.

A block diagram of the electronics used to readout the 8x8 detector array is shown in Figure 5. The performance of the readout system is determined largely by the hybrid preamplifiers which first amplify the signals from the 8x8 detector array. We chose to use a commercially available preamplifier array in our first prototype gamma camera. The preamplifiers (Lecroy HQV 820) are constructed in thick film hybrid technology and contain 8 channels of preamplifier in a single wide 24 pin dual inline package (DIP). The rated performance of the preamplifiers was not extraordinary and translates to about 5 keV FWHM of noise referenced to a CZT gamma spectrum. Despite these performance limitations, we chose the HQV 820 preamplifiers because they were the only multi-channel units available commercially. A circuit board was designed and built that

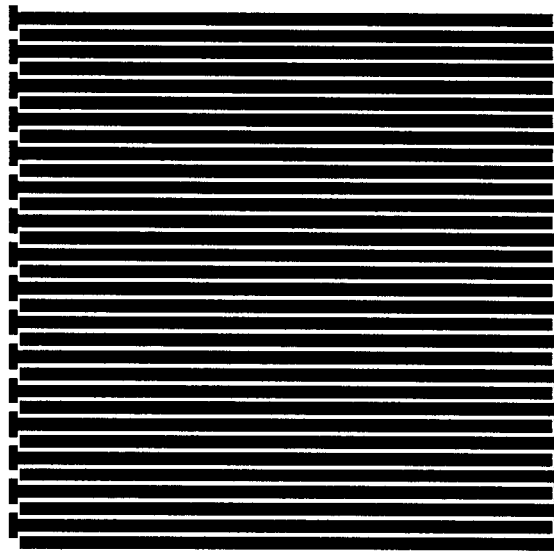
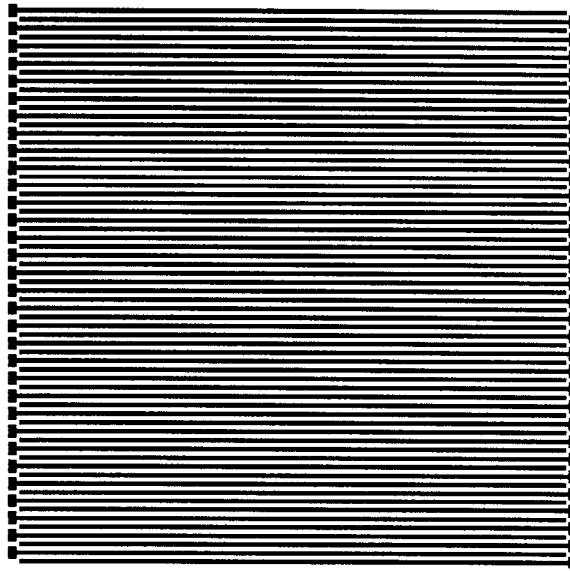


Figure 3. Photolithographic mask pattern used for fabricating two orthogonal strip detector designs. The upper part of the figure shows the metallization layout (mask pattern) for a 32x32 device intended for a 1.5 cm x 1.5 cm device design. The lower part of the figure illustrates a 16 x 16 device intended for use on a 1 cm² device. Several other devices were also designed (and later constructed) that are not depicted in this figure. The additional designs included: 64 x 64 patterns for 1.5 x 1.5 cm² detectors, 32 x 32 patterns for both 1.5 x 1.5cm² and 1.0x1.0 cm² devices, and 16 x 16 patterns for use on 1.5 x 1.5cm² and 1.0 x 1.0 cm² devices.

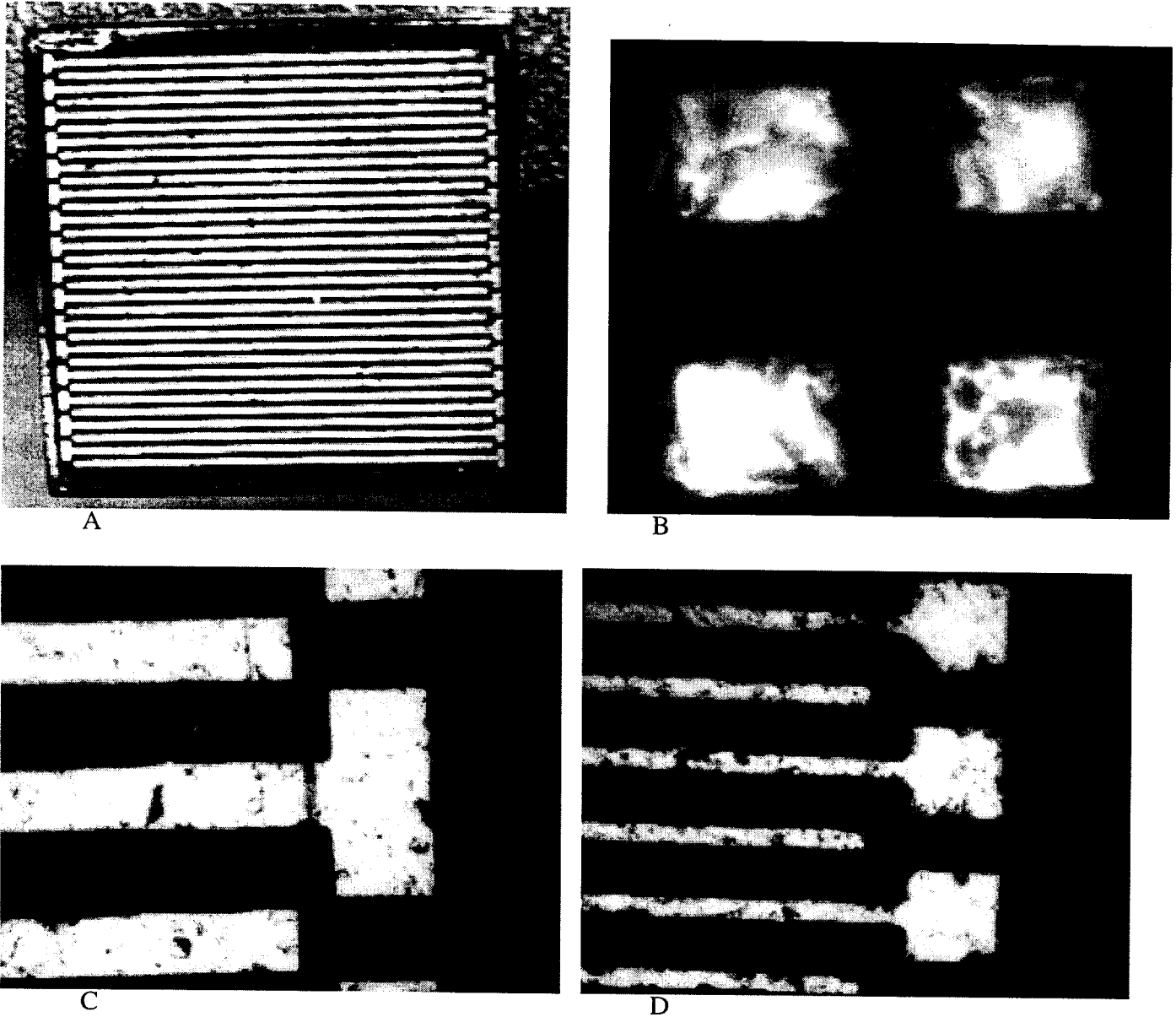


Figure 4. Photographs of high density strip detectors fabricated for gamma cameras. **A.** Photograph of an entire 32 x 32 orthogonal strip CZT detector. The CZT substrate has dimensions 15 mm x 15 mm x 2 mm. **B.** Infrared photomicrograph of a portion of a 32 x 32 CZT device. In the infrared the CZT substrate is transparent, but the gold contact strips are opaque; thus, a single detector pixel is the intersection of the dark bands in this photograph. **C.** Optical photomicrograph of a bond pad at the end of a strip on a 32 x 32 device. **D.** Optical photomicrograph of a bond pad at the end of a strip on a 64 x 64 device. The pitch (distance between strip centers) on this device is approximately 200 microns.

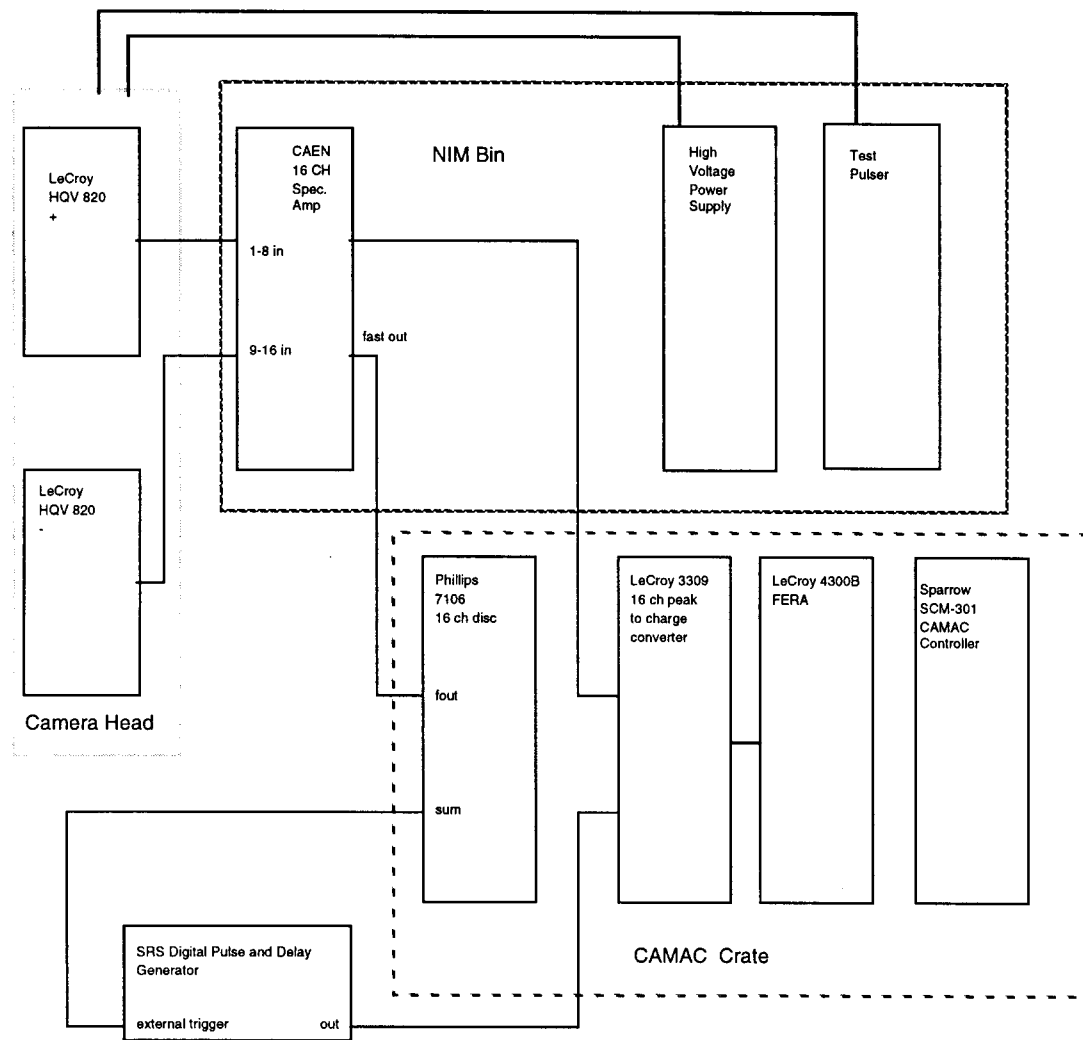


Figure 5. Block diagram of the electronic readout system used in the 8x8 gamma camera. The system may be viewed as consisting of two branches: one for counting hits (discriminator) and the other branch for spectroscopy (ADC). Pulses from the Lecroy HQV820 preamps in the camera head are shaped and amplified by a CAEN 16 channel spectroscopy amplifier, these pulses are then fed to both a 16 channel discriminator and to a 16 channel ADC. Triggering of a read cycle is initiated in hardware whenever at least two channels are above the discriminator threshold, subsequent event selection is then performed in software after the CAMAC discriminators and ADCs have been read.

accommodated two of the eight channel hybrid preamplifiers as well as the miscellaneous passive components to couple the detector to the preamplifier unit. The "front-end" circuit board containing the preamplifiers also contained a socket for holding an 8x8 detector. The additional capacitance and conductor trace length needed to socket the detectors would degrade the noise performance of the system somewhat, but we decided that the tradeoff of being able to test several detectors designs with the same readout circuit outweighed the slight performance degradation that socketing the detector induced. The front end circuit board was constructed of a Teflon derivative to minimize "1/f" noise that would be induced by a conventional circuit board containing glass additives. A photograph of the assembled circuit board is shown in Figures 6 with an 8x8 CZT detector attached.

The front-end electronics were housed in a separate chassis which comprised the "camera head" and was connected via coaxial cables to the remaining readout electronics. A photograph of the assembled camera head is shown in Figure 7. The remaining electronics were housed in NIM bins and a CAMAC crate and interfaced to the readout computer with a SCSI CAMAC controller. A form of sparse readout- implemented in hardware- was used to limit the amount of data the computer must obtain from the comparators and ADCs in the CAMAC crate. Signals from all 16 channels (8 columns and 8 rows, 64 pixels) were fed to a 16 channel comparator; when at least two comparators had fired, a master gate signal was triggered initiating the readout sequence. Additional event selection was also performed in software and is described in the next section of this report.

After some difficulty configuring the complex readout system of the 8 x 8 camera, we were able to get the electronics to perform adequately (see camera testing later in this report). The biggest deficiency found in the readout system during testing was the higher than anticipated noise level from the shaping amplifier stages. Normally the signal to noise ratio of a nuclear spectroscopy system is determined by the charge sensitive preamplifier- the first stage of amplification of the signal from the detector. After some analysis, however, we determined that the signal was being degraded by our sixteen channel spectroscopy amplifier. Further analysis- and consultation with the manufacturer of the amplifier (CAEN of Milan, Italy) indicated that the amplifier was performing according to specification, but it was designed for signals of larger magnitude than the preamplifier was producing (i.e. the charge gain of the preamplifier was too low; feedback capacitance too high). Despite these difficulties, the measured noise performance of the system was about 15 keV FWHM which is still very good, and suitable for simultaneous spectroscopy and position measurements.

After building the first generation gamma camera electronics (for reading out the 8x8 camera), it became apparent that commercially available nuclear electronics would be unsuitable for reading out high density strip detectors (> 16 x 16 strips) due to the expense and physical size of the readout electronics. In particular, the hybrid preamplifiers we used- which were the highest density commercially available- would consume too much space in a high density camera. For this reason we undertook an investigation of custom integrated electronics that would be more suitable for a camera readout. Eventually, we teamed with a group at Lawrence Berkeley National Laboratory (LBNL) who had developed an ASIC for reading out photodiodes in a scintillation camera. Together with the engineers at LBL, we modified the design of the photodiode readout chip to be compatible with the CZT and HgI₂ strip detectors we were building. The modified ASIC was then fabricated using the MOSIS fabrication service using the Hewlett Packard 1.2 micron CMOS process. The predicted performance of the new ASIC is better than 1 keV FWHM noise (referred to CZT) from each channel of the device. The ASIC provides 16 channels of charge sensitive preamplifier and sixteen channels of shaping amplifier in a 2.5 mm x 2.5 mm die. A photomicrograph of the ASIC we built is shown in Figure 8. As of this writing, the ASIC is undergoing testing and will be ready for deployment in an imaging system in the near future.

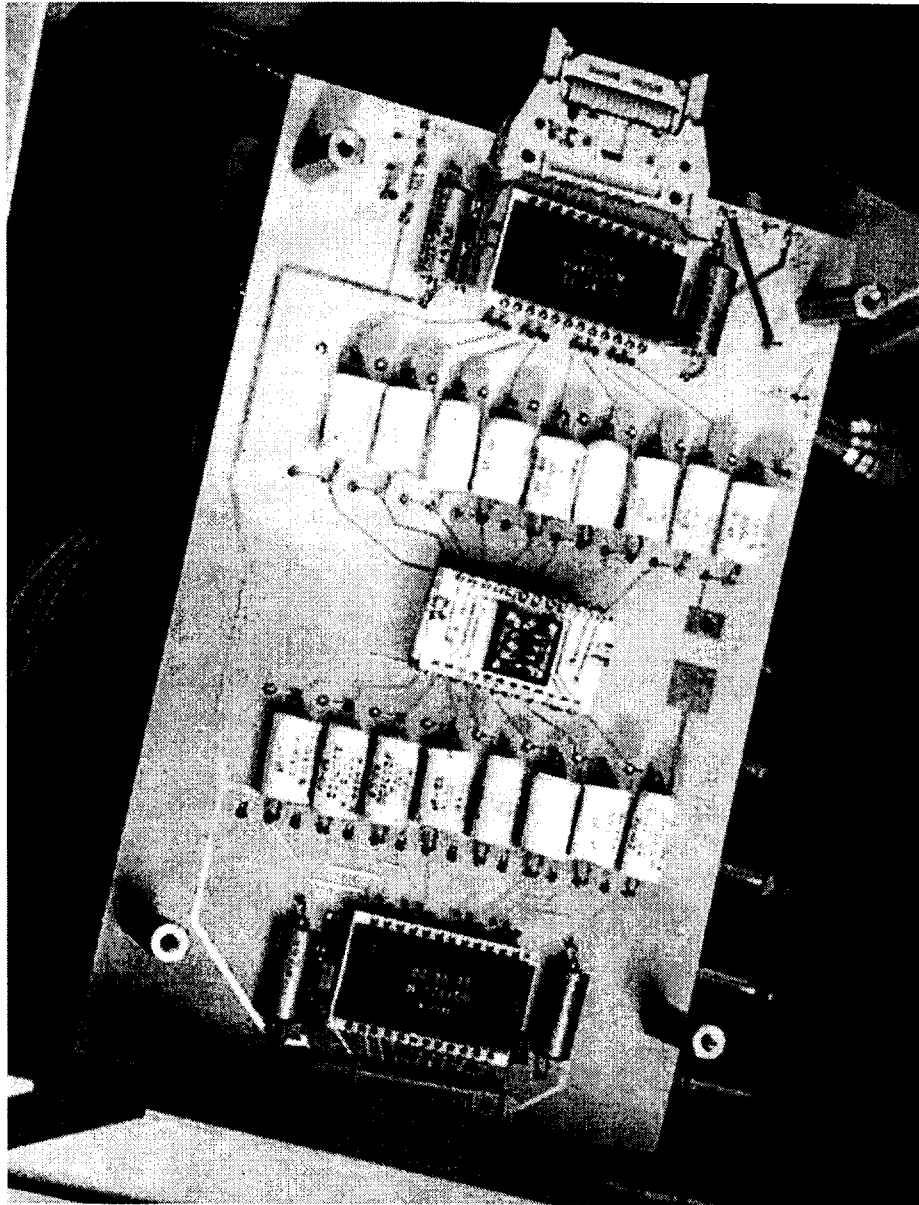


Figure 6. Photograph of the “front-end” circuit board used in the 8x8 gamma camera. An 8x8 CZT detector module mounted in a DIP socket is visible in the center of the photograph. The white cylindrical objects on either side of the detector module are the decoupling capacitors (an AC coupled configuration was used to connect the detector strips to the preamp). The black rectangular objects on either end of the circuit board are the eight channel preamplifier arrays. The circuit board was constructed from Duroid- a Teflon derivative- to minimize the “1/f” noise produced by the circuit traces between the detector and the preamplifier inputs.

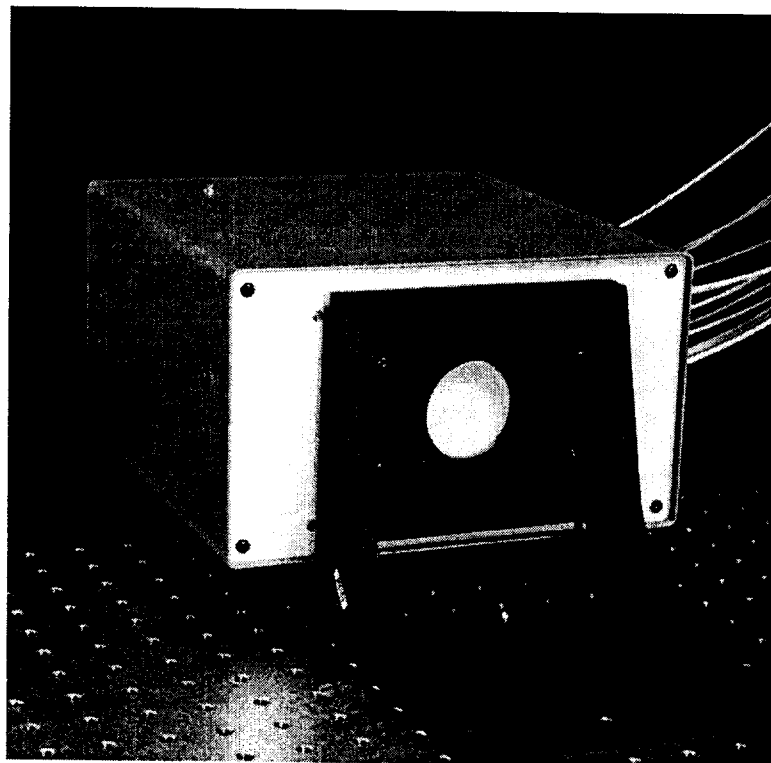
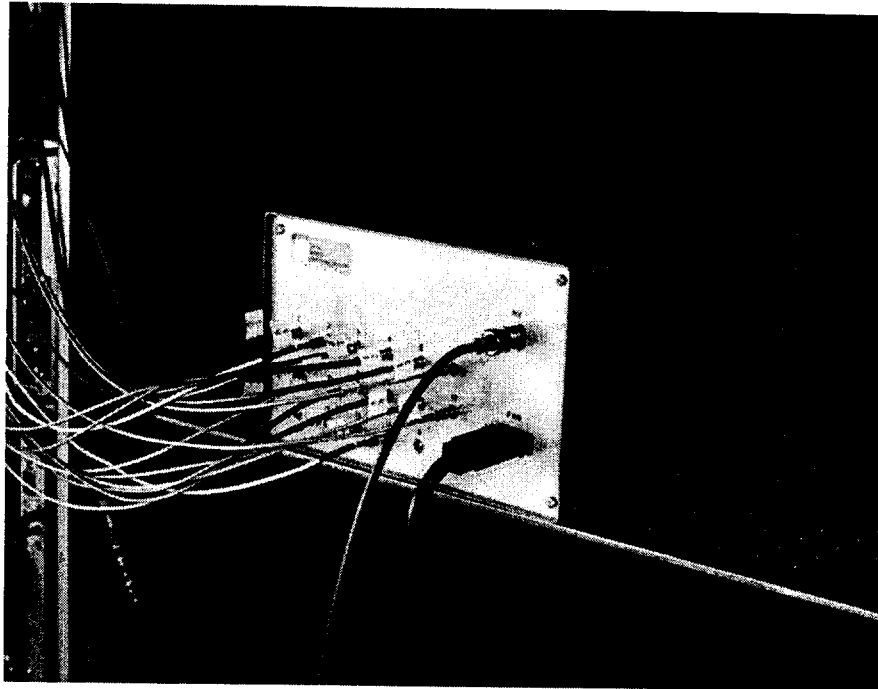


Figure 7. Photographs of the completed 8x8 gamma camera head. The upper photograph shows the interconnections to the back side of the camera: coaxial cables, high voltage cable for detector bias, and preamplifier power cables. The lower photograph shows the front of the camera attached to an optical table.

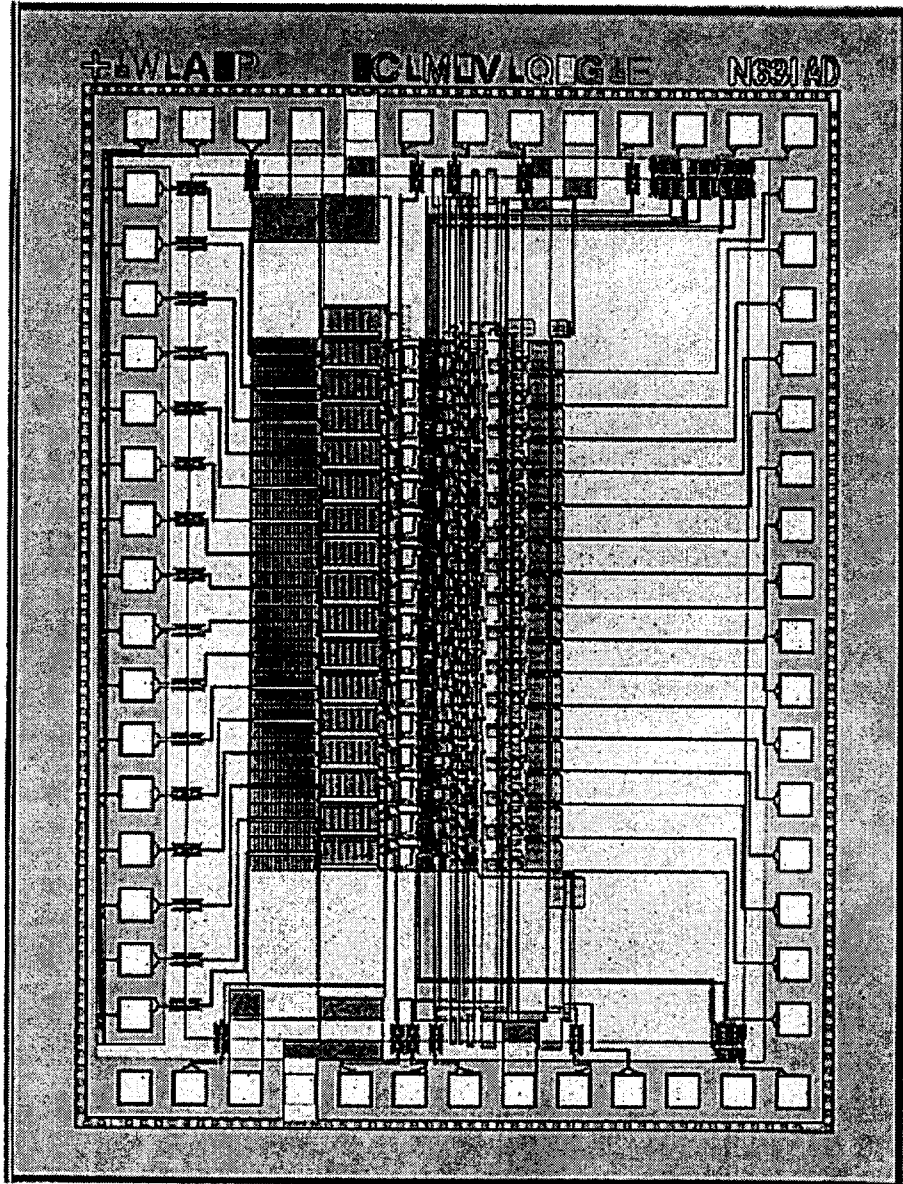


Figure 8. Photomicrograph of application specific integrated circuit (ASIC) developed to readout semiconductor strip detectors for gamma cameras. The ASIC die measures 2.5 mm x 2.0 mm and contains 16 charge sensitive preamplifiers, and 16 shaping amplifiers. The ASIC was developed in collaboration with researchers at Lawrence Berkeley National Laboratory.

Software

The final engineering component of the gamma camera to be developed during the program was the software used to readout the gamma camera. The software interrogated the ADCs and discriminators in the CAMAC crate, decoded the position of interaction on the orthogonal strip detector, and created pulse height spectra of the interactions that occurred at each pixel. Another function of the software was to provide real time feedback on the operation of the camera, and diagnostics of various camera functions (such as cross-talk between channels). The software was written in the high level control language "Kmax" to minimize development and reduce the amount of time spent writing low level CAMAC control routines. Figure 9 illustrates the graphical user interface (GUI) presented to the user when operating the software. The software, which executes on a Power Macintosh computer, also contains many more windows and dialog boxes than are shown in Figure 9, and can be called up for various diagnostic functions.

System Testing

To demonstrate the capabilities of imaging with room temperature semiconductor detectors, the gamma camera system described in the previous sections of this report was tested with isotopic sources. Three general types of experiments were performed with both HgI₂ and CZT detectors mounted in the gamma camera: flood field images of the detector plane to determine the uniformity of its response, imaging of objects with the aid of a pinhole collimator, and gamma-ray pulse height spectroscopy of sources.

Flood field images were obtained by mounting a ¹³³Ba source a few cm in front of the detector plane and recording the count rate at each pixel location as well as the energy spectrum of the source. Imaging studies were performed by mounting a pinhole collimator on the front of the gamma camera assembly and irradiating the collimator with isotopic sources. By configuring the collimator position such that the magnification of the source was unity, it was possible to measure the position resolution on the detector plane very easily by recording images of the source as it was moved in a plane parallel to the detector plane. Some results from such an experiment are shown in Figure 10.

Pulse height spectra were also acquired in both flood field mode and with the pinhole collimator. A typical pulse height spectrum taken with a HgI₂ detector is shown in Figure 11. Two components were identified in the broadening of the pulse height spectra: Gaussian broadening due to random electronic noise and an asymmetrical distortion of the gamma-ray peaks due to charge trapping effects. It was observed that significant variations existed between the pulse height spectra taken from different pixels on the device as well as large differences from device to device. It became clear in the course of our investigation that the uniformity of the material used to make the devices was an important factor in determining the performance of detectors made from these semiconductor crystals. This issue is discussed in more detail in the next section of this report.

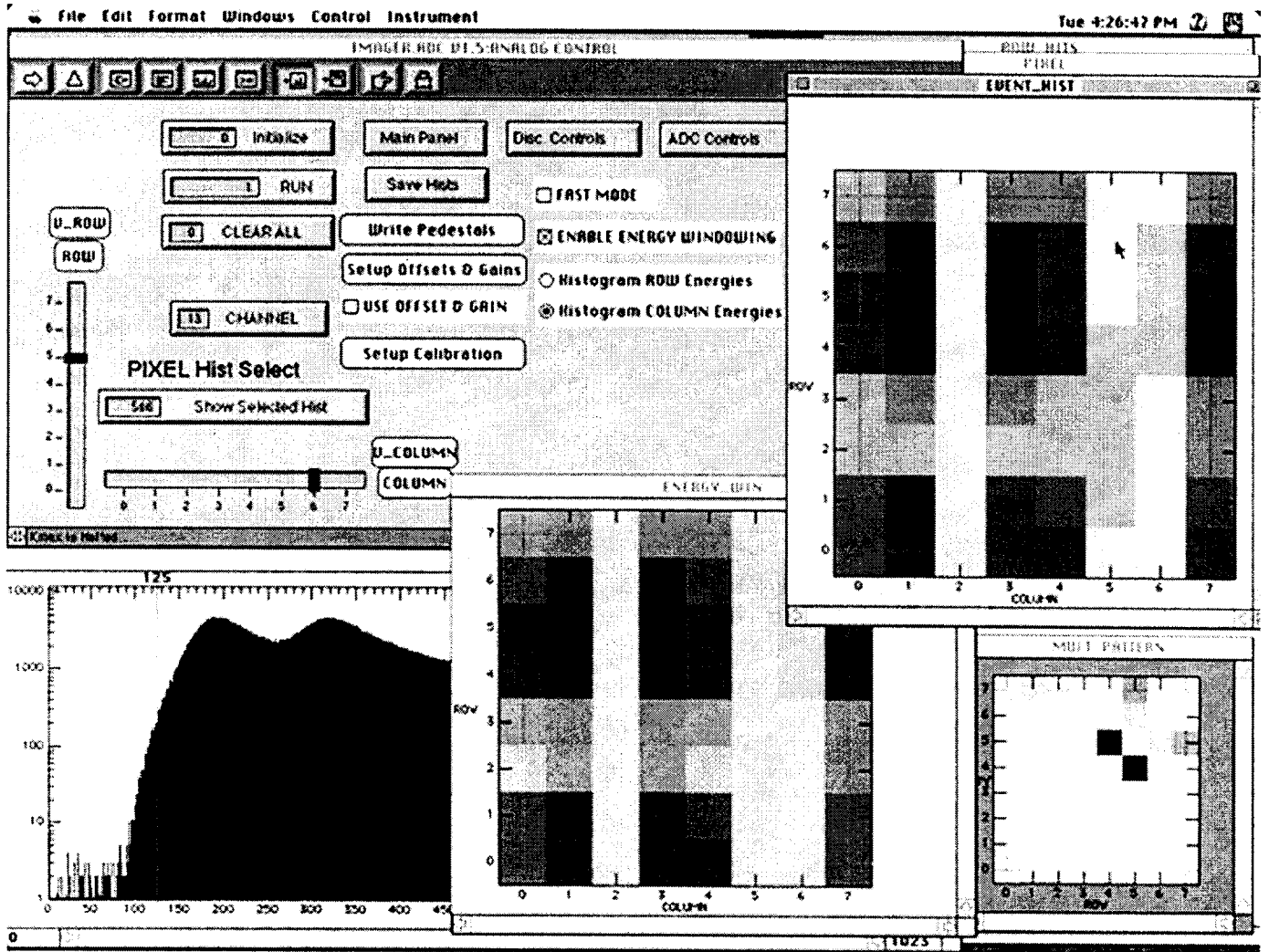


Figure 9. Printout of Graphical User Interface (GUI) of software for controlling the operation of the "8x8" gamma camera. A large number of windows and dialog boxes are available to the operator for controlling and monitoring the operation of the camera. The windows titled "EVENT-HIST" is a display of the total number of counts at each pixel. The window titled "ENERGY_WIN" is the display of intensity of hits that fall within a range of pulse height values selected on a master histogram of pulse height intensities.

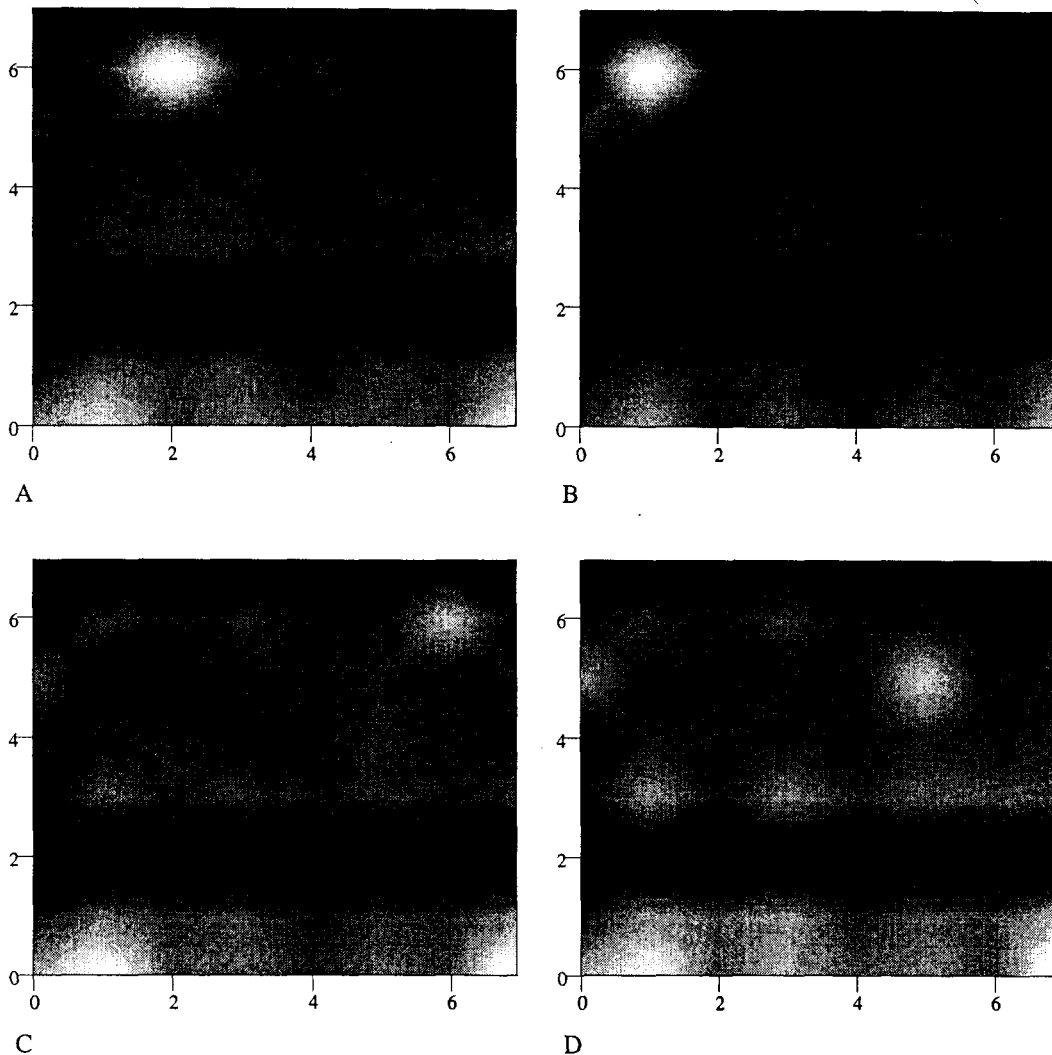


Figure 10. Images of a ^{133}Ba isotopic source taken with the 8x8 Camera and a pinhole collimator. Image A is the reconstructed gamma-ray intensity distribution (at the detector plane) of the source in its initial position. Image B depicts the intensity distribution when the source spot has been moved to the left 1.0 mm from its initial position. In Image C and D the source has been moved 4.0 mm to the right, and 3.0 mm right and 1mm down respectively. The dark stripe in the lower portion of the images is due to a malfunctioning strip. Note the non-uniformity of the “background” intensity (regions of the detector plane where there is little or no gamma illumination). This non-uniformity was probably due to two reasons: non-uniformity in the detector array itself, and variation in the noise level of each electronic readout channel. The variation in apparent background intensity due to electronic noise could be remedied by providing independent pulse discriminators for each channel, but the non-uniformity of the detector array could only be corrected through improved crystal substrate uniformity and/or device processing. These data demonstrate that our initial gamma camera prototype is capable of position sensitive detection of gamma rays with a spatial resolution of 1 mm or better.

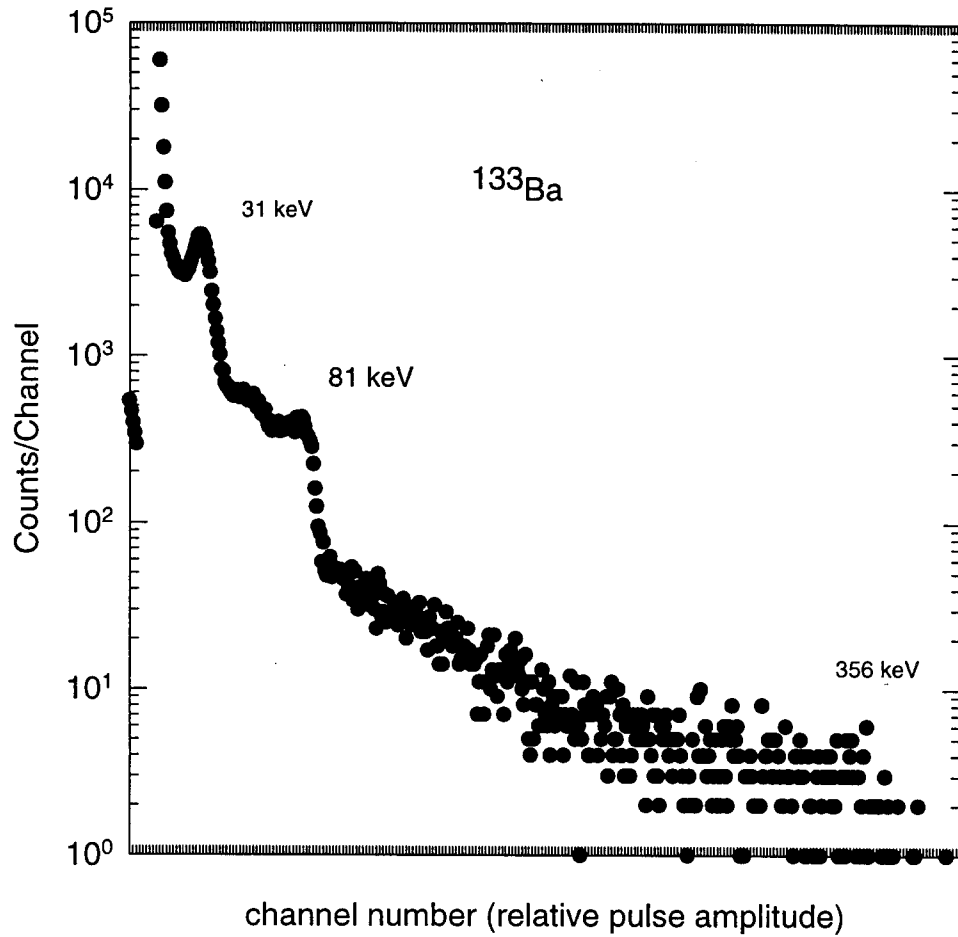


Figure 11. Pulse height spectrum obtained by irradiating a CZT 8x8 orthogonal strip detector with photons from a ^{133}Ba source. Lower energy photopeaks (~ 31 and ~ 81 keV) are clearly resolved and exhibit a Gaussian broadening due to the read-out electronics in the gamma camera. The higher energy photons emitted from ^{133}Ba (276, 302, 356, and 383 keV) are not clearly resolved due to “hole tailing” of the peaks from charge trapping in the CZT crystal.

Uniformity of Semiconductor Materials

Studies performed on the 1 cm² imaging detector developed in this program indicated that uniformity of the electrical properties of the crystals used to make the detectors was a serious concern. Furthermore, our interaction with the manufacturers of the crystals indicated that it was difficult to obtain crystals of these semiconductors in sizes much greater than about 1 cm² because of the larger scale uniformity of the crystalline boules from which the samples were cut. For these reasons we embarked on an examination of the uniformity of the physical and electrical uniformity of room-temperature semiconductor materials useful for radiation detectors. We focused our attention on measuring the uniformity of crystals of CZT, as these are the only room temperature semiconductor crystals available in large sizes (> 10 cm²), and would be the most likely material to be used in future larger area gamma cameras.

Figure 12 and Figure 13 illustrate some of the many results we obtained in our uniformity studies. Figure 12 shows a transmission IR map of one half of a 4 inch boule of CZT. Note the inhomogeneities that are clearly present in the crystal boule. Figure 13 illustrates a computer image of the leakage current obtained by scanning the same sample shown in the previous figure with apparatus designed and built at SNL/CA. These uniformity studies, and results we obtain from individual imaging detectors, clearly show that uniformity of the starting materials used to produce semiconductor imaging detectors is major issue limiting the development of larger imaging detectors, as well as the manufacturing yield of existing detectors.

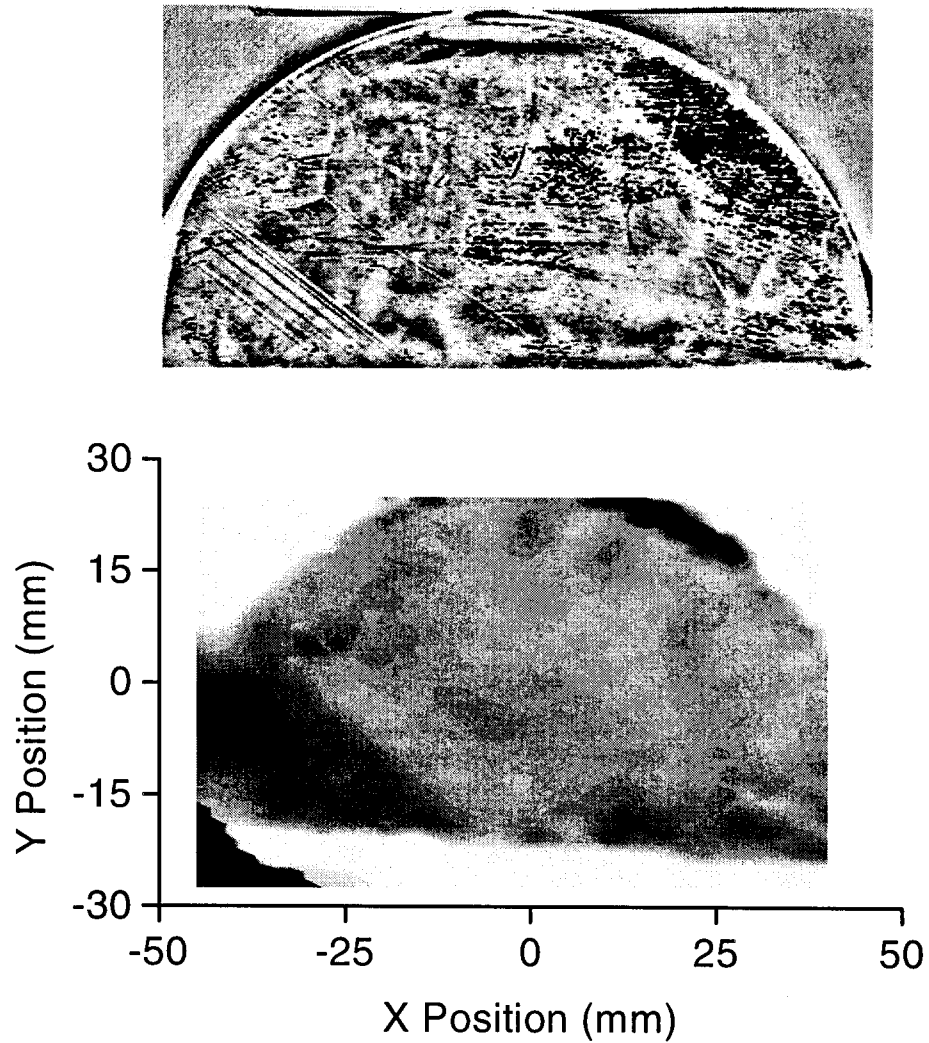


Figure 12. Results of spatial mapping studies on a CZT wafer. The upper part of the figure illustrates a an IR transmission photograph of a 4" diameter half wafer sliced from a CZT boule. The lower part of the figure depicts an intensity profile of the leakage current measured on the same sample with an automatic scanning apparatus designed for this purpose. Note the correlation between features in the IR photograph with the electrical measurements.

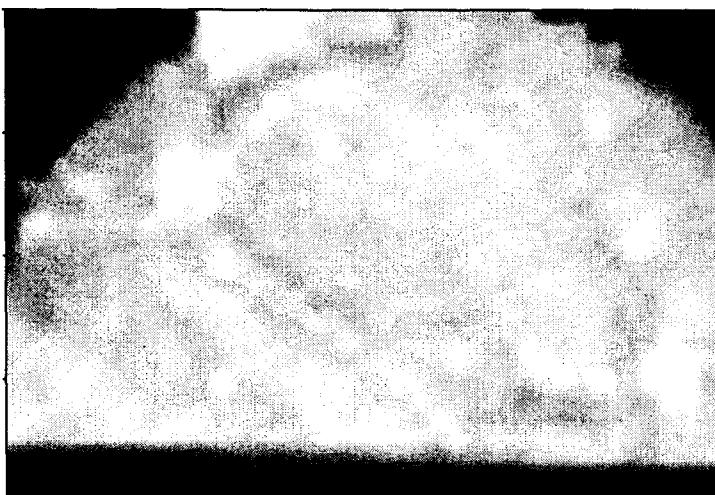


Figure 13. Results of gamma-ray detection uniformity studies taken on the same wafer shown in the previous figure. The wafer was irradiated with photons from a ^{133}Ba source. A probe was moved across the wafer under computer control and used to obtain a pulse height spectrum from each probed position. The upper figure illustrates the integrated intensity of counts in the pulse height spectra above 200 keV; the lower figure illustrates the corresponding intensity distribution for counts below 200 keV. Note the wide variation in observed count intensity across the wafer. These, and similar studies, indicate that the uniformity of the crystalline substrates used to manufacture gamma ray detectors from CZT will have to be improved before large area ($> 10 \text{ cm}^2$) imaging detectors can be produced from this material.

CONCLUSIONS

The goal of the project that was described in this report was to demonstrate the feasibility of using room-temperature semiconductor gamma ray detectors as the basis for a new generation of radiation imaging systems. We succeeded in this goal by completing research tasks in the areas of position sensitive radiation detector design and construction, multi-channel electronic readout design, software for image data acquisition and image reconstruction, and ,finally, measurement of the uniformity of the electrical and physical properties of semiconductor samples.

We conclude from this research that this technology is very promising and should be pursued vigorously in the future. It is very likely that miniature gamma-cameras based on the technology described in this report will play a major role in future radiation imaging systems for nuclear medicine, treaty verification and fingerprinting stored weapon pits. Perhaps the biggest barrier we identified to the rapid evolution of this technology is the quality of the currently available semiconductor materials used to fabricate these devices. In particular, we found that the uniformity of the semiconductors used to fabricate these detectors must be improved if larger area commercial devices will be constructed for localizing cancerous tumors.

REFERENCES

1. W. R. Willig, *Nucl. Instrum. Methods* **96**, 615 (1971).
2. J. P. Ponpon, R. Stuck, P. Siffert, B. Meyer, and C. Schwab, *IEEE Trans. Nucl. Sci.* **NS-22**, 182 (1975).
3. A. J. Dabrowski, W. M. Szymczyk, J. S. Iwanczyk, J.H. Kusmiss, W. Drummond, and L. Ames, *Nucl. Instrum. Methods* **213**, 89 (1983).
4. H. L. Malm, T.W. Raudoff, M. Martina, and K. R. Zanio, *IEEE Trans. Nucl. Sci.* **NS-20**, 500 (1973).
5. See, for example, the review by R. C. Whited and M. Schieber, *Nucl. Instrum. Methods* **162**, 119 (1979).
6. B. V. Novikov and M.M. Pimonenko, *Fiz. Tekh. Poluprovodn.* **4**, 2077(1970) [*Sov. Phys. Semicond.* **4**, 1785 (1970)]
7. J. C. Muller, A. Friant, and P. Siffert, *Nucl. Instrum. Methods* **150**, 97(1978).
8. R. B. James, X. J. Bao, T. E. Schlesinger, J. M. Markakis, A. Y. Cheng, C. Ortale *J. Appl. Phys.* **66**, 2578 (1989).
9. I. Ch. Schluter and M. Schluter, *Phys. Rev. B.* **9**, 1652 (1974).
10. T. Goto and A. Kasuya, *J. Soc. Jpn.* **50**, 520 (1981).
11. R. C. White and L. van den Berg, *IEEE Trans. Nucl. Sci.* **NS-24**, 165 (1977).
12. M. Schieber, H. Hermon, and M. Roth, in *Semiconductors for Room-Temperature Radiation Detector Applications*, Materials Research Society Symposium Proceedings **302**, 347 (1993).

APPENDIX A

Publications Resulting from this Work

Gamma Ray Imaging and Spectroscopy System Using Room-Temperature Semiconductor Detector Elements

J.C. Lund¹, N.R. Hilton², J.E. McKisson³, J.M. Van Scyoc⁴, H. Hermon¹, R.W. Olsen¹,
and R.B. James¹

¹Sandia National Laboratories, Livermore CA 94551

²University of Arizona, Tucson AZ 85724

³RTI, Inc., Alachua, FL 32615

⁴University of California, Los Angeles, CA 90024

Abstract

We report on the design, construction, and testing of a gamma-ray imaging system with spectroscopic capabilities. The imaging system consists of an orthogonal strip detector made from either HgI₂ or CdZnTe crystals. The detectors utilize an 8x8 orthogonal strip configuration with 64 effective pixels. Both HgI₂ or CdZnTe detectors are 1 cm² devices with a strip pitch of approximately 1.2 mm (producing pixels of 1.2 mm x 1.2mm). The readout electronics consist of parallel channels of preamplifier, shaping amplifier, discriminators, and peak sensing ADC. The preamplifiers are configured in hybrid technology, and the rest of the electronics are implemented in NIM and CAMAC with control via a Power Macintosh computer. The software used to readout the instrument is capable of performing intensity measurements as well as spectroscopy on all 64 pixels of the device. We report on the performance of the system imaging gamma-rays in the 20-500 keV energy range and using a pin-hole collimator to form the image.

*Corresponding author, full address and contact information:

Jim Lund

M.S. 9405

Sandia National Laboratories

PO Box 969, Livermore, CA 94551

email: jlund@sandia.gov

phone: 510-294-3871

fax: 510-294-3870

Introduction

Devices for imaging the spatial distribution of gamma-ray emitting isotopes- gamma cameras- have been in wide use in nuclear medicine for many years and currently represent a commercial annual market of several billion US dollars. Gamma cameras are potentially useful in non-medical applications as well; in fields such as non destructive evaluation of dense materials, and imaging of stored high-level radioactive waste. The conventional gamma camera employed in a hospital today consists of an Anger camera¹; a device consisting of an array of photomultiplier tubes (PMTs) attached to a large (approximately 1.0 meter in diameter) crystal of inorganic scintillating material such as NaI(Tl) or BGO. When a gamma-ray photon interacts with the scintillating crystal in a gamma-camera, it produces an energetic electron via a photoelectric or Compton scattering process. The energetic electron produced by gamma ray interaction subsequently deposits its energy within a millimeter or so of the gamma-ray interaction site. When the electron loses its energy it produces scintillating photons which are detectable by the PMTs. By determining the position centroid (Anger logic) of the light detected from several PMTs, the position of interaction of the photon can be determined. The scintillators used in conventional gamma cameras require some tens of eV of energy deposited to produce a single scintillating photon. Thus only a few tens of optical photons are produced per keV of energy deposited by the gamma ray. This low number of photons- or more accurately the statistical fluctuation in this number of photons- ultimately determines both the energy and position resolution of the detector used in existing gamma camera systems. The resolution with which a gamma-camera can encode position on the detector is not the same as the spatial resolution with which the gamma camera system can estimate the position of the gamma ray emitter. The position resolution of the collimator is also an important factor; in general, the position resolution in the resultant image is the convolution of the spatial response function of

the collimator and the spatial response function of the detector. In modern large gamma cameras, the position resolution of the system is usually determined by the collimator. However, in a portable system employing a high resolution collimator (such as a pinhole collimator), the system resolution would be determined by the position resolution of the detector plane. Under these circumstances (i.e. portable gamma-cameras) the position resolution of the gamma ray imager may be limited by the scintillator /PMT detector. Furthermore, if one seeks to determine the isotope that is producing gamma ray emission, the ability to resolve isotopes is limited by the energy resolution of a scintillator based detector system.

An obvious method for overcoming the limitations of scintillator based systems is to use a semiconductor detector based gamma camera. In a semiconductor detector, only a few eV are required to produce an electron-hole pair. Furthermore, the generation of the charge pairs in a semiconductor detector is a sub-Poissonian process (fluctuation is less than a random process), resulting in a lower theoretical limit for the energy resolution of the detector, and potentially better position resolution as well. Indeed, semiconductor gamma ray spectrometers made from germanium long ago displaced scintillation systems as the best detection technique for energy spectroscopy. However, because of the cryogenic cooling involved, it is often not practical to use a germanium detector particularly for field use. Instead, one solution to producing improved miniature gamma-cameras is to use room temperature semiconductor materials (such as HgI₂ and CZT) to build the detectors. In this paper we describe the design, construction and testing of such a semiconductor gamma camera..

System Design

There are several approaches that might be tried to produce a semiconductor detector with imaging capabilities. The most obvious solution is to configure a square array of individual

detector elements into the desired image plane. However, since a typical imager could require a square array of dimensions 32 x 32 elements (1024 total elements), it is not economical to fabricate and assemble into an array such a large number of individual elements.

The next most obvious approach is to fabricate a monolithic array of individual detector elements on a single semiconductor substrate. If lithographic approaches to fabrication are used, it becomes practical to fabricate monolithic arrays with a suitable number of elements, however reading out the signal from such an array would require very complex electronics. In general, to readout an $N \times N$ array of individual pixels requires N^2 separate channels of readout electronics; for arrays larger than about 4x4 this becomes a very complex solution, particularly since each channel of electronics must be very high performance (low noise) to take advantage of the benefits of semiconductor detectors.

An alternative approach to reading out a semiconductor detector array was first proposed by Gerber et al² and is known as an orthogonal strip design. Such an approach is illustrated in **Figure 1** and consists of rows of parallel electrical contacts (strips) placed at right angles to each other on opposite sides of the detector. By making use of the temporal coincidence between events recorded on both sides of the detector, it is possible to readout an effective array of N^2 effective detector elements using only $2N$ channels of readout electronics. The orthogonal strip approach was used for all of the detectors described in this paper.

Detector Design and Fabrication

Detectors were designed and built using both HgI₂ and CZT materials as substrates. Our first detectors were 8x8 devices fabricated on HgI₂ and CZT substrates approximately 2.0 mm thick. These 8x8 orthogonal strip detectors resulted in devices with 64 effective pixels with each pixel a

square of approximately $0.125 \times 0.125 \text{ cm}^2$ dimensions. These devices were placed on chip carriers (see **Figure 2**) that allowed them to be plugged directly into the readout electronics.

Detectors were fabricated by evaporating metal contacts on to the surface of etched crystal substrates using a shadow mask to define the strip pattern. A total of four detectors were fabricated: three from CZT and one from HgI_2 . The detectors were mounted on standard 24 pin alumina dual in-line packages (DIPs) commonly used for hybrid electronic circuits. Fine gold wires ($25 \text{ }\mu\text{m}$ diameter) were bonded to the metal contact strips using silver epoxy, the other end of the wire was then bonded to a metal foil pattern on the alumina substrate of the dual inline package. The packaged detectors could then be inserted directly into a socket on the front-end readout circuit board. Subsequent testing of the detectors indicated that all of the detectors operated correctly as spectroscopic imaging devices, however, in three of the four devices (1 HgI_2 , and 2 CZT) there was one strip that did not function. As of this writing it is not clear if the cause of the strip failure was in the detector or in the bonding and interconnection used to connect the detector to the readout electronics. The remaining CZT detector was fully functional (all rows and column strips functioned).

Electronic Readout

The system used to readout the 8×8 detector arrays made use of hybrid preamplifiers followed by NIM and CAMAC readout amplifiers and ADCs. A block diagram of the electronics used to readout the 8×8 detector array is shown in **Figure 3**. The performance of the readout system is determined largely by the hybrid preamplifiers which first amplify the signals from the 8×8 detector array. We chose to use a commercially available preamplifier array in our first prototype gamma camera. The preamplifiers (Lecroy HQV 820) are constructed in thick film hybrid technology and contain 8 channels of preamplifier in a single wide 24 pin dual inline

package (DIP). The rated performance of the preamplifiers translates to about 5 keV FWHM of noise referenced to a CZT gamma spectrum. We chose the HQV 820 preamplifiers because they were the only multi-channel units available commercially.

A circuit board was designed and built that accommodated two of the eight channel hybrid preamplifiers as well as the miscellaneous passive components to couple the detector to the preamplifier unit. The "front-end" circuit board containing the preamplifiers also contained a socket for holding an 8x8 detector. The additional capacitance and conductor trace length needed to socket the detectors would degrade the noise performance of the system somewhat, but we decided that the tradeoff of being able to test several detector designs with the same readout circuit outweighed the slight performance degradation that socketing the detector induced. The front end circuit board was constructed of a Teflon derivative to minimize "1/f" noise³ that would be induced by a conventional electronic circuit board. A photograph of the assembled circuit board is shown in **Figure 4** with an 8x8 CZT detector attached.

The front-end electronics were housed in a separate chassis which comprised the "camera head" and was connected via coaxial cables to the remaining readout electronics. The remaining electronics were housed in NIM bins and a CAMAC crate and interfaced to the readout computer with a SCSI CAMAC controller. A form of sparse readout- implemented in hardware- was used to limit the amount of data the computer must obtain from the comparators and ADCs in the CAMAC crate. Signals from all 16 channels (8 columns and 8 rows, 64 pixels) were fed to a 16 channel comparator; when at least two comparators had fired, a master gate signal was triggered initiating the readout sequence. Additional event selection was also performed in software.

Software

In order to readout the coincident signal from the strip detector, decode the pixel position, and visualize the gamma ray intensity distribution at the detector plane it was necessary to write software to control the gamma camera. The software interrogated the ADCs and discriminators in the CAMAC crate, decoded the position of interaction on the orthogonal strip detector, and created pulse height spectra of the interactions that occurred at each pixel. Another function of the software was to provide real time feedback on the operation of the camera, and diagnostics of various camera functions (such as cross-talk between channels). The software was written in the high level control language "Kmax" to minimize development and reduce the amount of time spent writing low level CAMAC control routines. Figure 5 illustrates the graphical user interface (GUI) presented to the user when operating the software. The software, which executes on a Power Macintosh computer, also contains many more windows and dialog boxes than are shown in Figure 5, and can be called up for various diagnostic functions.

Results

To demonstrate the capabilities of imaging with room temperature semiconductor detectors, the gamma camera system described in the previous sections of this report was tested with isotopic sources. Three general types of experiments were performed with both HgI₂ and CZT detectors mounted in the gamma camera: flood field images of the detector plane to determine the uniformity of its response, imaging of objects with the aid of a pinhole collimator, and gamma-ray pulse height spectroscopy of isotopic sources.

Flood field images were obtained by mounting a ¹³³Ba source a few cm in front of the detector plane and recording the count rate at each pixel location as well as the energy spectrum of the source. Imaging studies were performed by mounting a pinhole collimator on the front of the gamma camera assembly and irradiating the collimator with isotopic sources of small active

diameter. It was then possible to measure the position resolution on the detector by recording images of the source as it was moved in a plane parallel to the detector plane. Some results from such an experiment are shown in **Figure 6**.

Pulse height spectra were also acquired in both flood field mode and with the pinhole collimator. A typical pulse height spectrum taken with a CZT detector is shown in **Figure 7**. Two components were identified in the broadening of the pulse height spectra: Gaussian broadening due to random electronic noise³ and an asymmetrical distortion of the gamma-ray peaks due to charge trapping effects^{4,5}.

Discussion

An instrument which imaged and performed spectroscopy on gamma-rays was designed built and tested. The imaging system used a room temperature semiconductor detector made from either CZT or HgI₂. All detectors fabricated for this study were approximately 1.0 cm² in active area and were of an 8x8 orthogonal strip design (64 effective pixels). Reliability problems with the detectors were experienced; only one of four detector units was fully functional, but all detector units were partly functional (15 out of 16 strips were functional on the remaining three devices). It is not clear- as of this writing- the cause of the non-functional strips.

Simple tests of the position resolution of the detector elements indicated that the CZT and HgI₂ strip orthogonal strip detectors were capable of resolving the movement of a point source on the imaging plane with a resolution of better than 1.0 mm. Further testing will be required to better quantify the spatial resolving capabilities of this instrument. The ability of the imaging detectors to resolve the energy of the detected gamma rays was also measured. It was found that energy resolution- as measured by pulse height spectroscopy- was limited at low energies by electronic noise at approximately 15 keV FWHM. At higher gamma ray energies, the energy resolution was

limited by hole trapping and extensive “hole-tailing” was observed on the low energy sides of the peaks. This behavior was expected, and is consistent with the performance of single element detectors made from these materials.

Despite the deficiencies observed in the performance of our first system, we found our results (and those obtained by others using similar methods) to be quite encouraging. Orthogonal strip detectors made from room-temperature semiconductor detector materials appear to be a viable method for imaging the distribution of radionuclides with high spatial resolution and good energy resolution; particularly if the hole trapping effects in these detector materials can be minimized.

We are currently working on improving the performance of our gamma-ray imaging devices by making use of electron-only device designs (analogous to the gridded ion chambers used with gas detectors^{6,7}) to minimize hole tailing, and using an custom integrated circuit readout chip to reduce the electronic noise and increase the number of readout channels.

Acknowledgments

We gratefully acknowledge support of this project by Laboratory Directed Research and Development (LDRD) funds (#3514.090).

References

1. H.O. Anger, *Gamma Ray Detection Efficiency and Image Resolution in Sodium Iodide*, 35, p. 693, (1964).
2. M.S. Gerber, D.W. Miller, P.A. Schlosser, J.W. Steidley, and A.H. Deutchman, *Position Sensitive Gamma Ray Detectors Using Resistive Charge Division Readout*, IEEE Trans. Nuc. Sci, NS-24, p. 182, (1977).
3. V. Radeka, *Low-Noise Techniques in Detectors*, Ann. Rev. Nucl. Part. Sci., 38, p. 217, (1988).

4. R.O. Bell, *Calculation of Gamma-Ray Pulse Height Spectrum in a Semiconductor Detector in the Presence of Charge Carrier Trapping*, Nucl. Inst. and Meth., **93**, p. A2, (1971).
5. W. Akutagawa and K. Zanio, *Gamma Response of Semi-Insulating Material in the Presence of Trapping and Detrapping*, J. Appl. Phys., **40**, p. 3838, (1969).
6. G.F. Knoll, **Radiation Detection and Measurement**, 2nd ed., Wiley, New York, (1989).
7. O. Frisch, British Atomic Energy Report, **BR-49** (1944).

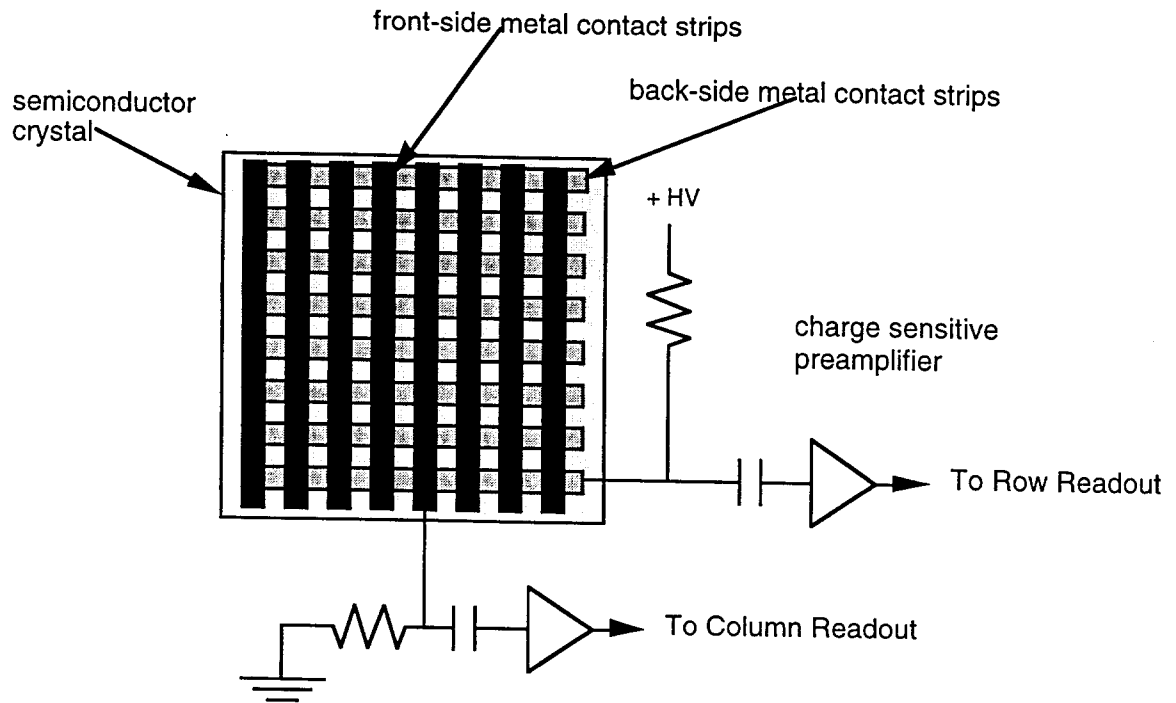


Figure 1. Diagrammatic view of an “8x8” orthogonal strip detector and front-end readout electronics. The metal contact strips are deposited on opposite sides of a square piece of semiconductor wafer. Event localization on the detector plane is determined by scoring a coincidence event between a column and a row. Using this method reduces the complexity of the readout electronics considerably. In general, to readout an array of N^2 effective pixels only requires $2 \times N$ channels of readout electronics, as opposed to N^2 channels of readout required for a detector consisting of an array of individual pixels.

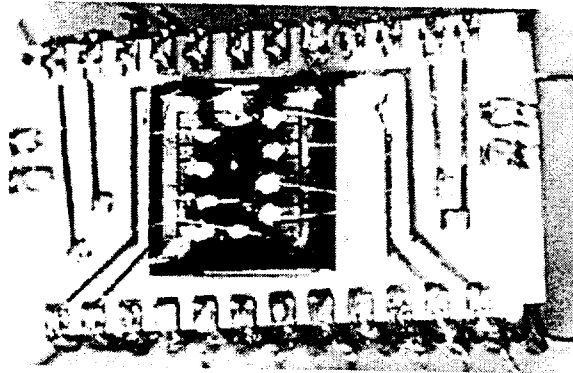


Figure 2. Photograph of an 8x8 orthogonal strip CZT detector mounted on a ceramic 24 pin DIP package.

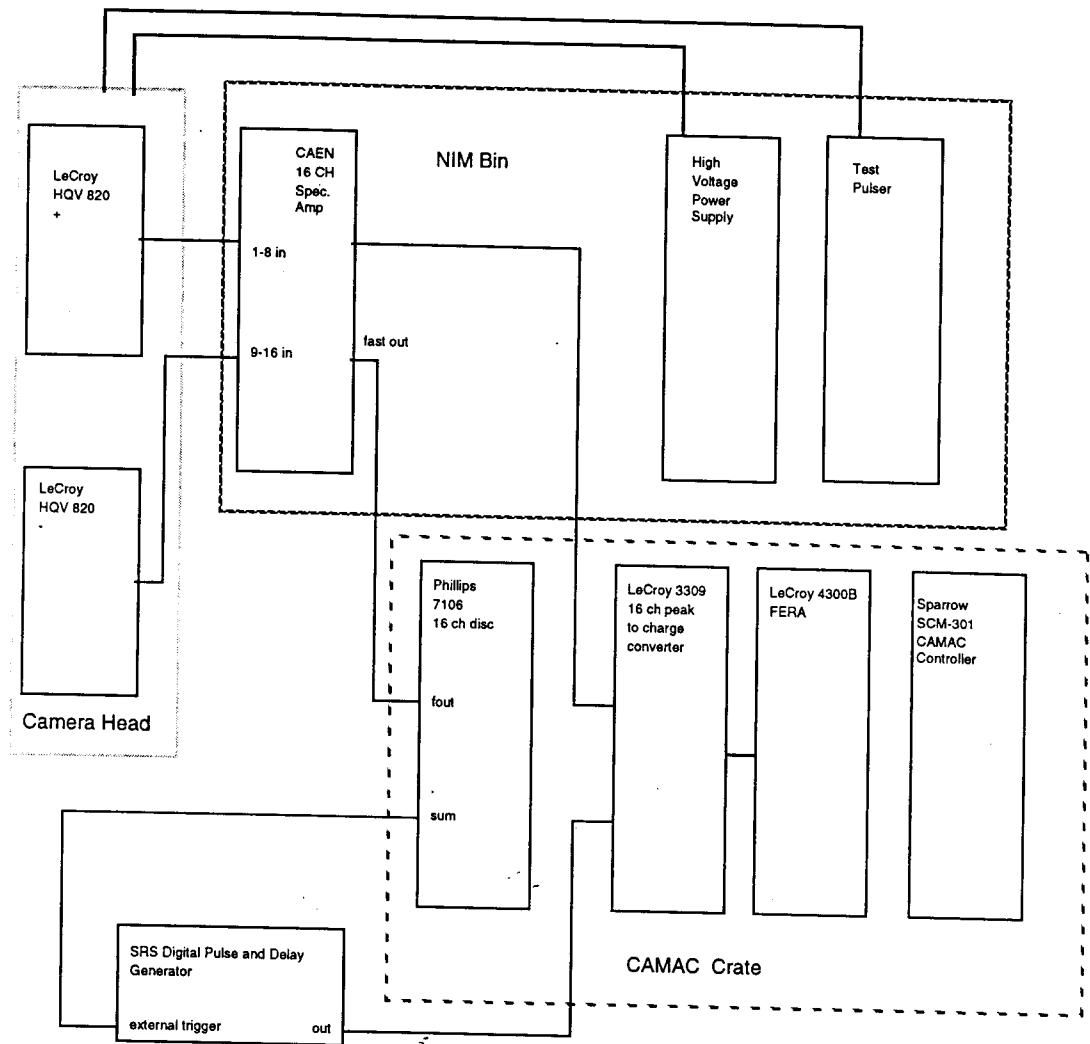


Figure 3. Block diagram of the electronic readout system used in the 8x8 gamma camera. The system may be viewed as consisting of two branches: one for counting hits (discriminator) and the other branch for spectroscopy (ADC). Pulses from the Lecroy HQV820 preamps in the camera head are shaped and amplified by a CAEN 16 channel spectroscopy amplifier, these pulses are then fed to both a 16 channel discriminator and to a 16 channel ADC. Triggering of a read cycle is initiated in hardware whenever at least two channels are above the discriminator threshold, subsequent event selection is then performed in software after the CAMAC discriminators and ADCs have been read.

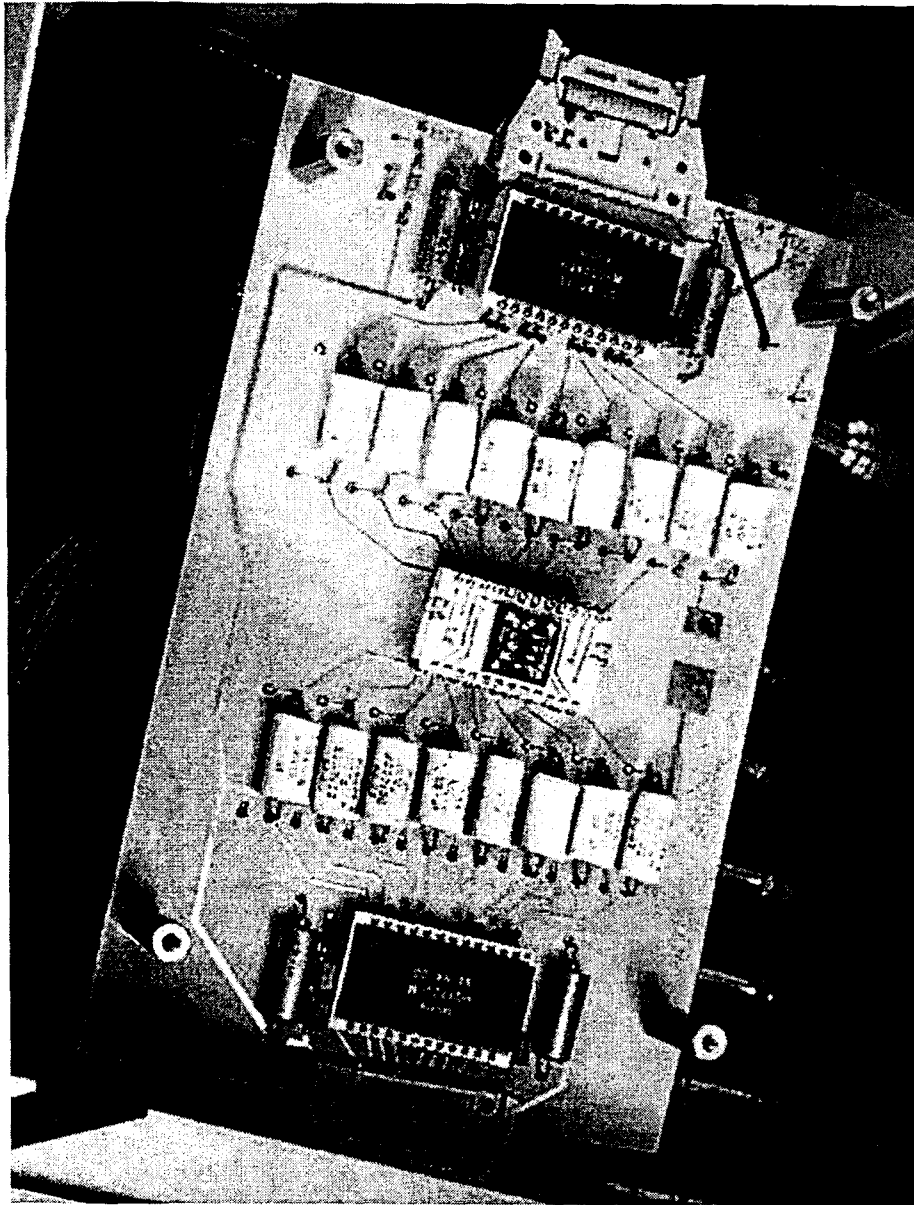


Figure 4. Photograph of the “front-end” circuit board used in the 8x8 gamma camera. An 8x8 CZT detector module mounted in a DIP socket is visible in the center of the photograph. The white cylindrical objects on either side of the detector module are the decoupling capacitors (an AC coupled configuration was used to connect the detector strips to the preamp). The black rectangular objects on either end of the circuit board are the eight channel preamplifier arrays. The circuit board was constructed from Duroid- a Teflon derivative- to minimize the “1/f” noise produced by the circuit traces between the detector and the preamplifier inputs.

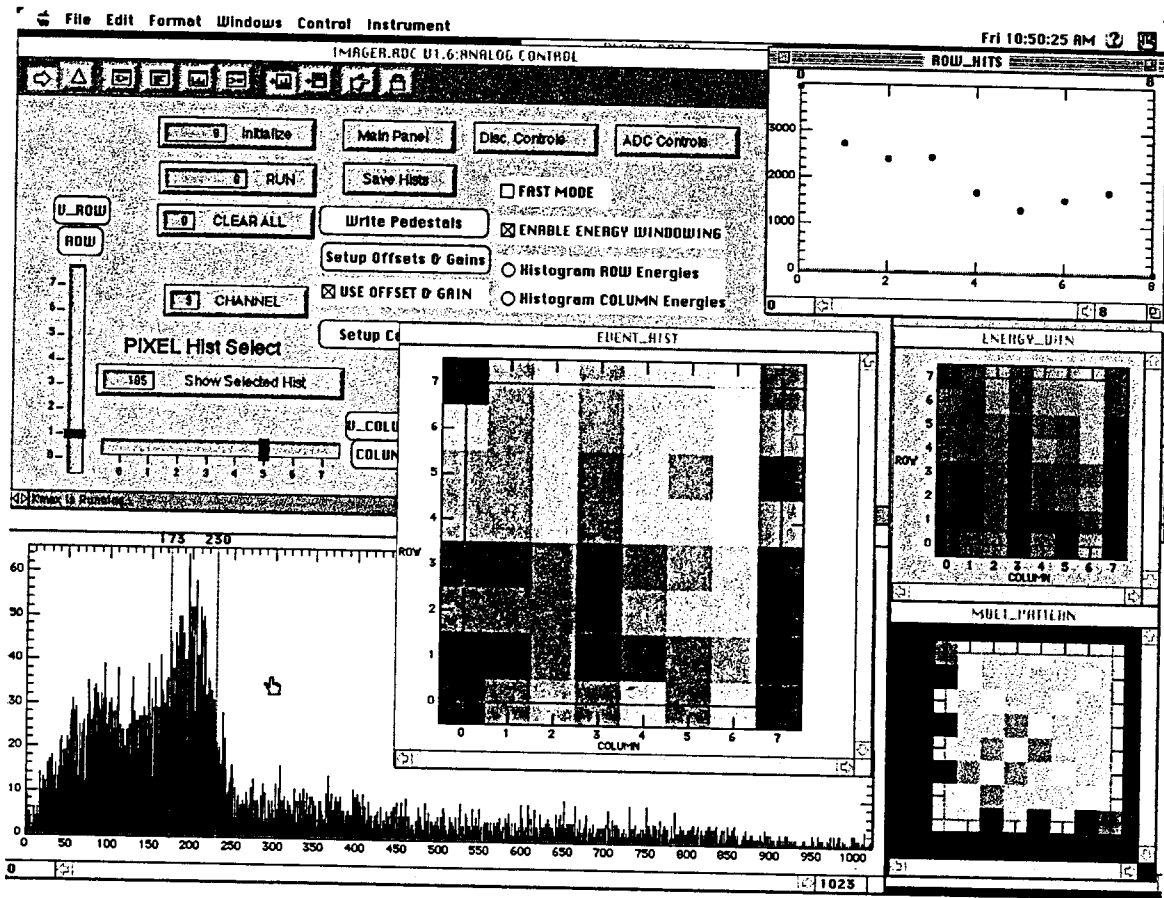


Figure 5. Printout of Graphical User Interface (GUI) of software for controlling the operation of the "8x8" gamma camera. A large number of windows and dialog boxes are available to the operator for controlling and monitoring the operation of the camera. The windows titled "EVENT-HIST" is a display of the total number of counts at each pixel. The window titled "ENERGY_WIN" is the display of intensity of hits that fall within a range of pulse height values selected on a master histogram of pulse height intensities.

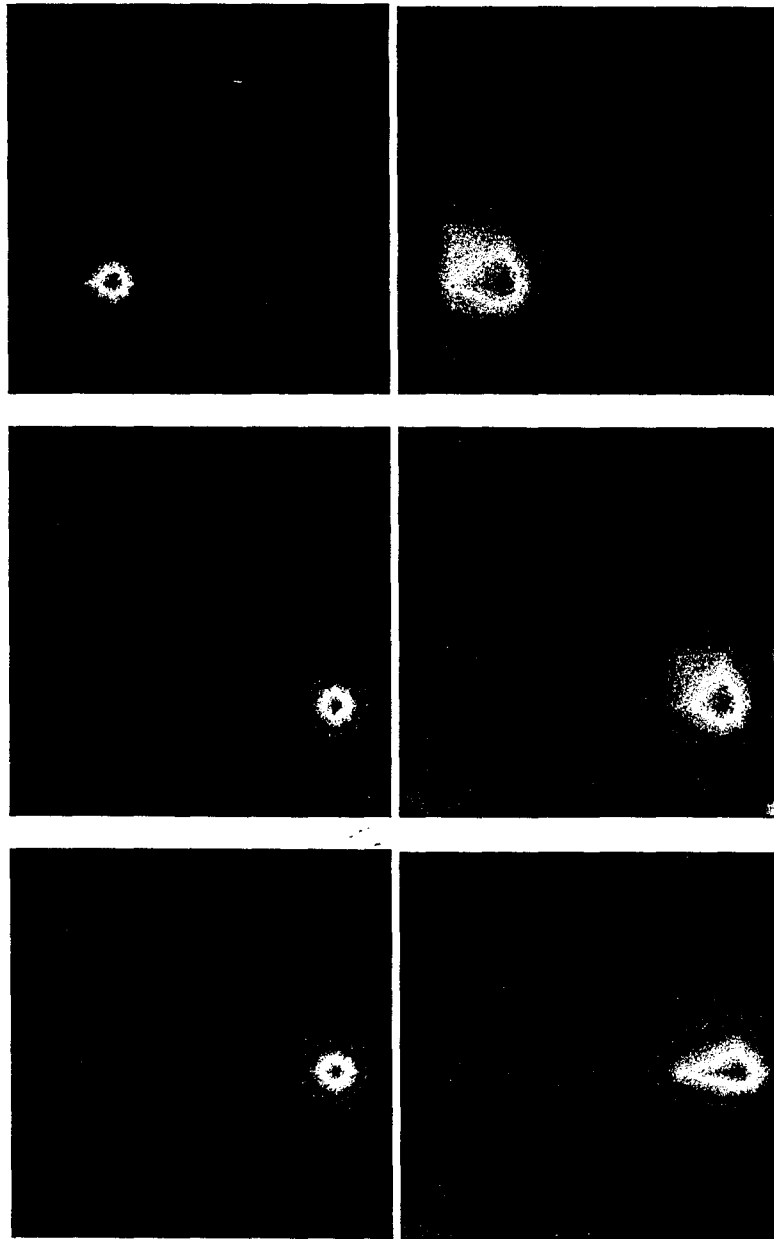


Figure 6. Contour plots of the intensity distribution of the gamma-ray count rate on a CZT orthogonal strip detector. These images were formed by a pin-hole lead collimator placed between the detector and the ^{133}Ba source. The images on the right are composed of raw data sorted into spatial bins by the data collection software. The images on the left are filtered versions of the raw data; a simple cut-off filter was used (at 50% of maximum image intensity) to reject counts below the cut-off. The source is located at an initial position in the uppermost images, the image of the source on the detector plane source was then moved to the right 3.75 mm and the middle images were produced. Finally, the source was moved again (up 1.25 mm) and the lowermost images obtained. These data imply that the spatial resolution at the detector plane is better than 1.0 mm.

Semiconductor Material Requirements for Orthogonal Strip Detectors

J.C. Lund^{1*}, H. Yoon², N.R. Hilton³, B.A. Brunett⁴, and R.B. James¹

¹Sandia National Laboratories, Livermore, CA 94551-0969

²Department of Materials Science and Engineering, University of California Los Angeles, L.A, CA 90095

³Department of Physics, University of Arizona, Tucson AZ 85724

⁴ Department of Electrical and Computer Engineering, Carnegie Mellon University, Pittsburgh, PA 15213

Abstract

We discuss the physical and electrical properties of semiconducting crystals necessary for use in orthogonal strip detectors. We also compute what constraints the properties of existing CdZnTe crystals place on the design of orthogonal strip detectors. First we consider the constraints imposed by uniform material that has limited charge carrier transport properties and resistivity. Next, we consider what effects spatially varying electrical properties (non-uniformities) have on the performance of detectors. Finally, we discuss the properties of CZT crystals available today that we have measured in our laboratory, and what ramifications these measured properties have on the design and construction of orthogonal strip detectors.

Keywords: Cadmium zinc telluride, orthogonal strip detectors, charge transport, gamma-ray imaging.

Introduction

Historically orthogonal strip detectors have been fabricated from germanium¹ which- when cryogenically cooled- has excellent charge transport properties and very low free carrier concentration. Recently, there has been a great deal of interest in the use of orthogonal strip detectors made from room-temperature semiconductor materials for applications in astronomy and medical imaging; with particular interest in detectors fabricated from CdZnTe (CZT). However, limitations in the charge transport properties, and resistivity of CZT crystals impose restrictions on the design of orthogonal strip detectors. Furthermore, crystals of CZT available today grown by the high pressure Bridgman method are not uniform in their electrical and physical properties and this imposes further restrictions on the design of orthogonal strip detectors made from this material.

Gross mechanical properties

Before we begin our detailed discussion of the electrical properties of CZT crystals it is first useful to briefly review the mechanical properties of CZT crystals as these properties influence the fabrication methods used to create orthogonal strip detector systems, and- to some degree- influence the range of conditions under which a detector can be stored or operated. For example, the hardness of the material may be relevant during the wire bonding process of fabricating pixel or strip detectors for imaging devices. Thermal conductivity may be an issue for devices operating with cooling (such as thermoelectrically cooled devices), and the thermal expansion coefficient may influence the choice of substrate materials or other surfaces bonded to the CZT crystal (particularly in situations where fluctuations in environmental conditions may occur, such as in space-flight). Table I shows a comparison of these material parameters among Si, GaAs, CdTe, and ZnTe. Although the incorporation of Zn into CdTe matrix enhances the mechanical and thermal properties, CdZnTe is roughly an order of magnitude worse in both categories compared to Si. In general, the mechanical properties of CZT - while not as robust as silicon or GaAs, are such that detectors can be fabricated and packaged without undue care, and methods developed to cut and polish silicon and GaAs crystals would be expected to work reasonably well with CZT. However, special care should be exercised in fabricating CZT strip detectors to avoid breaking or chipping of samples as CZT wafers are more prone to breaking than GaAs or silicon.

*Further author information:

Jim Lund

phone: 510-294-3871

fax: 510-294-3870

email: jlund@sandia.gov

| | Si | GaAs | CdTe | ZnTe |
|--|------------------------|------------------------|------------------------|------|
| Hardness (Knoop) (relative scale) | 1150 | 750 | ~100 | ~130 |
| Coefficient of Thermal Expansion (K ⁻¹) | 2.6 x 10 ⁻⁶ | 6.9 x 10 ⁻⁶ | 4.6 x 10 ⁻⁶ | |
| Thermal Conductivity (Wcm ⁻¹ K ⁻¹) | 1.4 | 0.5 | 0.07 | 0.1 |

Table I. Comparison of the mechanical hardness and thermal conductivity among Si, GaAs, CdTe, and ZnTe. Values obtained from Zanio², and Sze³

Electrical Requirements for Strip Detector Operation

In this section we consider what effect the electrical parameters of a *perfectly homogenous* crystal of CZT would have on the behavior of orthogonal strip detectors constructed from such a crystal. The case of the uniform crystal is a useful base-line to establish before we consider the more complicated case of real crystals which tend to have spatially non-uniform electrical characteristics.

As with any radiation spectrometer, the properties of the material used to construct an orthogonal strip detector must be such that the signal is large and does not vary with the interaction position within the device, and- equally important- that the noise level be well below that of the signal produced by an interaction. The factors that effect the size of the signal produced by radiation interaction in a crystal are the average energy required to create a charge pair in the material and the charge transport properties of the crystals. The average energy required to create a charge pair in a CZT crystal, ϵ_{pair} , is about 5.0 eV and is weakly dependent on the composition, x in the Cd_{1-x}Zn_xTe crystal. The value for ϵ_{pair} - as with other semiconductor detectors- is quite favorable and statistical fluctuations in the number of charge carriers would not be expected to degrade the energy resolution significantly.

The second factor that affects the size of the signal induced on the strips of a detector is the charge collection efficiency, η , the ratio of the charge induced on the contact to the charge created by an ionizing event. If the drift length of both electrons and holes always greatly exceeds the dimensions of the detector, the charge collection will be everywhere unity and there will be little if any distortion in the pulse height spectrum due to charge collection effects (this case is very nearly attained with germanium and silicon detectors). Unfortunately, in CZT crystals available today, the drift length of holes is usually much less than the useful detector dimensions and the drift length of electrons is often comparable to the detector dimensions. Generally, any semiconductor radiation detector that relies on the motion of both electrons and holes will produce good pulse height spectra up to approximately 100 keV, and then the energy resolution will be severely degraded due to "hole tailing" effects. Hole tailing is a severe asymmetrical broadening of the peaks in the pulse height spectrum due to differences in charge collection from different depths of photon interaction in the semiconductor detector.

To get undistorted pulse height spectra at higher photon energies, it is necessary to use some device design that relies only on the motion of electrons in the device, such as a "small pixel" device or perhaps a variation of a coplanar detector^{4,5}. Even for a perfect "electron only" device, the trapping of electrons can impose a significant constraint on device design. In the following, we compute what the magnitude of this constraint is for CZT material available today.

Although it can be a difficult computation problem to estimate the charge collection effects in an electron only device for all parts of the device volume, we can generalize to say that most devices would be expected to have weighting functions⁶ that are very localized to the electron collecting contact. Under these conditions, a signal is induced only when electrons make it close to the contact before they are trapped. An approximate rule for device design then, is to keep the maximum transit time to the collecting contact for electrons to be less than 0.3 μs . We typically measure the trapping lifetime of electrons in presently available CZT to be approximately 3 μs ; thus after only about 300 ns we would expect 10% of the charges to be trapped. The time taken for an electron to travel a particular trajectory depends on the line integral of the electric field along that trajectory. However, if we assume that the maximum field in a particular strip detector is perpendicular to the surface of the device and is no smaller than 10³ V we arrive at a maximum useful spectrometer thickness of only about 3 mm for presently available CZT (assuming an electron mobility of 1000 cm²V⁻¹s⁻¹). This maximum thickness is much less than would be desired for efficient operation of the detector with photons of energy greater than 200 keV.

Electrical properties related to Noise level

In addition to the broadening induced by charge collection in different regions of the detector, the other factor that determines the energy resolution in an orthogonal strip detector is the electronic noise. Electronic noise produces a purely Gaussian broadening in the pulse height spectrum accumulated by the strip detector. In the following section we present a quantitative model for estimating the noise in an orthogonal strip detector. We present this model to accomplish our original objective (to estimate what constraints material characteristics apply to device design), but- of course- this noise model can also be used by a strip detector designer to estimate the performance of a particular design.

We will consider two components in the noise model of an orthogonal strip detector: parallel and series white noise. We will ignore 1/f noise components because we feel they are influenced more strongly by non-detector factors (although 1/f noise can be an important factor in system performance). The key to developing a quantitative noise model of an orthogonal strip detector is to determine the current drawn by each strip (I_{strip}) and the capacitance of each strip (C_{strip}). Computing I_{strip} and C_{strip} can, in general, be a very difficult problem in a strip detector. To do a precise job of estimating leakage current and strip capacitance, it would be necessary to solve Laplace's (or Poisson's if trapped charge is significant) equation for the particular geometry in question. Although some excellent work has been done in developing approximate, analytic solutions to Laplace's equations for strip detectors^{7,8}, the results of these approximations are series of transcendental functions which can be tedious to compute results with, particularly in the early stages of device design when a large number of alternatives are under consideration. Instead of computing the capacitance and leakage current for each strip precisely, we will use simple expressions that express the lower and upper bounds of these values and use these values to compute the minimum and maximum noise of a particular device. However, these expressions are only valid for cases where the strips are all set to the same potential. If it is desired to combine a strip detector with a coplanar configuration (i.e. strips set to different potentials), it will be necessary to use a more sophisticated approach to estimating I_{strip} and C_{strip} .

Our approach to approximating the noise in CZT strip detectors will be to express the noise equations in terms of the effective area of the contacts. Then, the lower and upper bounds of the noise can be computed based on a lower and upper bound for the effective area of the device. Generally, we can assume that the minimum effective area of the strip is equal to the area of the metal that defines a strip and that the maximum effective area of a strip will be equal to the total device area divided by the number of strips. With these definitions, we can now estimate the two major detector noise contributions (parallel and series white) and deduce what influence material properties have on noise.

The detector's contribution to the parallel white noise will be given by the shot noise generated by leakage current of the strip :

$$ENC_{\text{parallel white}} = (I_{\text{strip}} A_3 \tau / q)^{1/2} \quad (1)$$

where q is the charge on the electron, τ is the time constant of the shaping amplifier, A_3 is a constant that depends on the definition of the shaping time and the form of the shaping amplifier's transfer function (e.g., Gaussian or triangular; the reader should refer to the paper by Gatti et al on the subject⁹). Where I_d be re-written for a an Ohmic device:

$$I_{\text{strip}} = V A_{\text{eff}} / \rho d \quad (2)$$

where A_{eff} is the effective area of the strip and d is the thickness of the detector. These results are expressed in traditional units of equivalent noise charge, ENC (rms electrons, or the standard deviation of the noise in electrons). To convert to the keV FWHM units more familiar in pulse height spectroscopy multiply ENC by 2.3 (to convert sigma to FWHM) then by 5×10^{-3} keV/electron (the average energy required to create a charge pair in CZT). If we assume a reasonable value for the resistivity of presently available CZT crystals is $1 \times 10^{11} \Omega\text{cm}$, and if we further assume that our average electric field in the detector (V/d) is $1 \times 10^3 \text{ Vcm}^{-1}$ we can estimate the detector's contribution to the parallel noise as a function of device area, such a plot is shown in **Figure 1**.

The detector's contribution to the series white noise may be written as

$$ENC_{\text{series white}} = (C_{\text{strip}}/q)(A_1 \gamma 2kT/\tau g_m)^{1/2} \quad (3)$$

where gamma is a numerical constant (~ 0.7)^{10,11}, g_m is the transconductance of the input field effect transistor (FET), and C_{strip} is the capacitance of the strip. We have assumed in Equation 3, that the input capacitance of the FET is the same as the strip capacitance and there is no stray capacitance. As before, we can use A_{eff} to compute the capacitance of the strip (using a parallel plate model). We recommend using- as a base-line- the ratio of the transconductance to input capacitance of a 2N4416 type n-channel JFET at the input (mho/pF) and assuming the FET could be scaled to match the strip capacitance. Using these assumptions, we have plotted the detector contribution to the series white series noise generated by a strip detector and plotted it in **Figure 2**.

Finally, we can calculate the total noise contributed by the detector by summing in quadrature the series and parallel components. An estimate of the total noise per strip is shown in Figure 3.

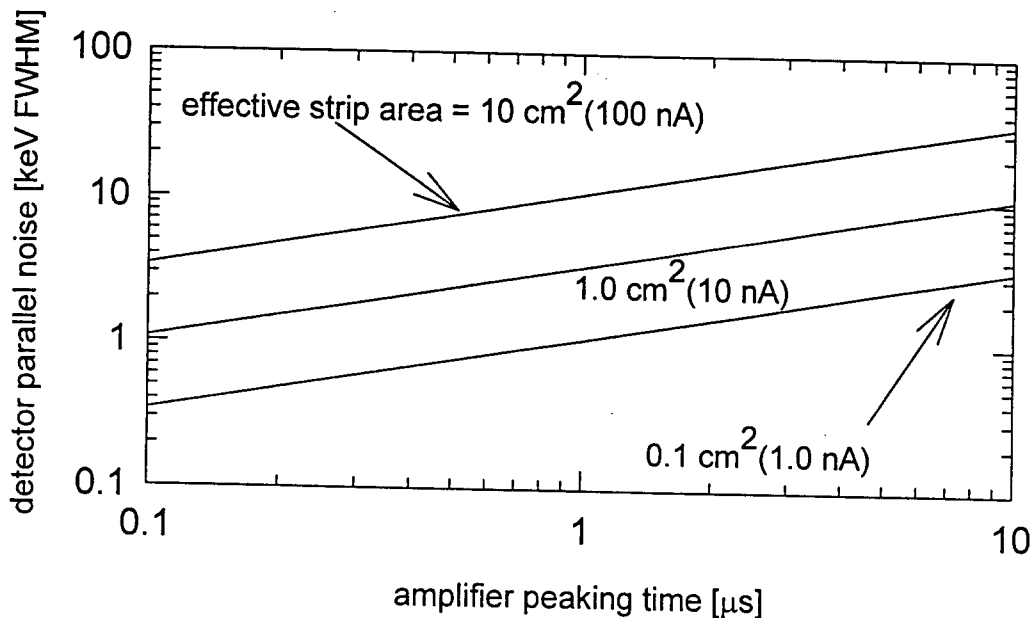


Figure 1. Detector contribution to parallel white noise as a function of amplifier peaking time for three different effective strip areas (and the leakage current associated with each strip). It was assumed that the CZT detector was 3.0 mm thick, operated at 300 V, had a mobility of $1000 \text{ cm}^2\text{V}^{-1}\text{s}^{-1}$, a resistivity of $1.0 \times 10^{11} \text{ Ohm cm}$ and that a Gaussian shaping amplifier was used. These calculations indicate that shot noise should not be a limiting factor in determining the resolution of an orthogonal strip detector if all of the strips on each side of the detector are at the same potential. However, if a coplanar detector design is used (strips at unequal potential) the shot noise may be much larger for a given strip area.

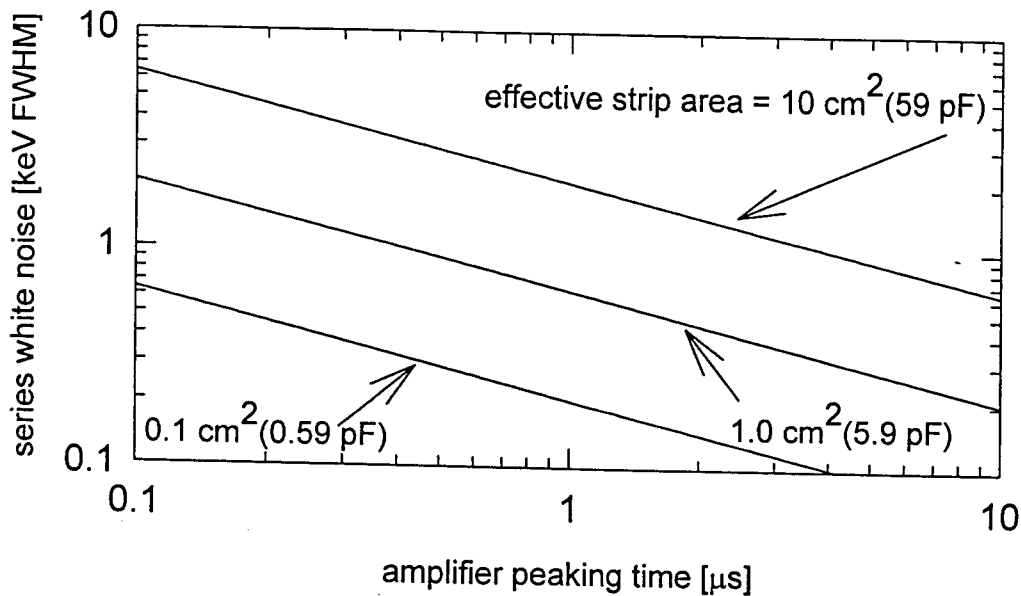


Figure 2. Detector contribution to the series white noise as a function of amplifier peaking time for three different effective strip areas (and the capacitance associated with each strip). It was assumed that the CZT detector was 3.0 mm thick that a Gaussian shaping amplifier was used. It was further assumed that there was no stray capacitance between the detector and input FET, that the input capacitance of the FET was always equal to the strip capacitance, and that the transconductance of the FET was equal to 2.4 mS pF^{-1} .

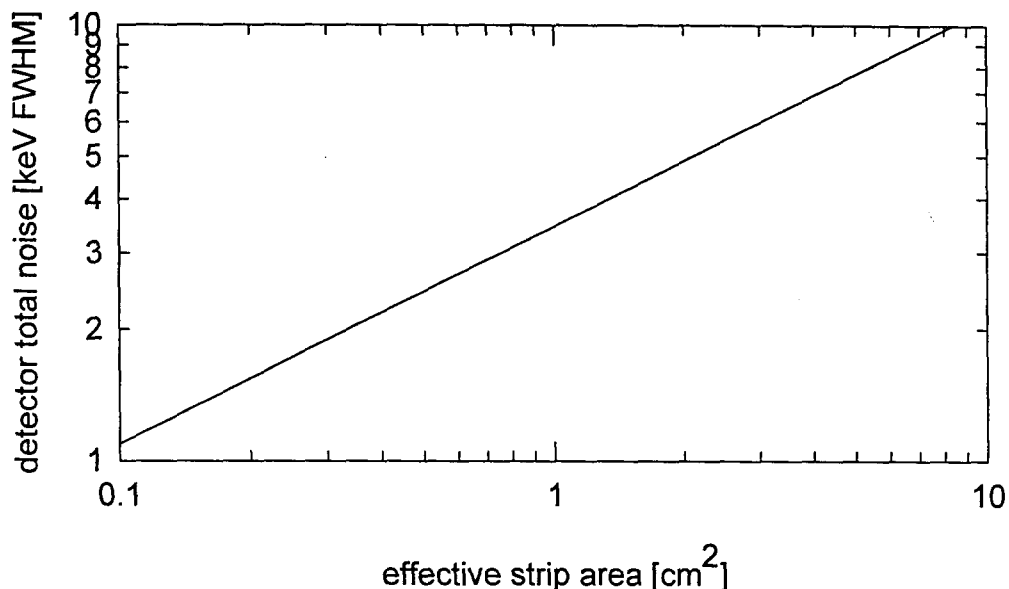


Figure 3. Detector contribution to the total noise in an orthogonal strip detector as a function of effective strip area. It was assumed that the CZT detector was 3.0 mm thick, operated at a bias of 300 V and that a Gaussian shaping amplifier was used with a peaking time of 1.0 μ s.

Examination of **Figure 3** indicates the influence of material properties on electronic noise is small. If existing material were perfectly homogenous we could - in principle- construct a detector 100 cm² in total area and composed of 100 x 100 orthogonal strips yet have an energy resolution of about 3 keV; fairly impressive performance. However, if it was desired to decrease the detector noise even further, the material properties that would have to be improved would be the resistivity (it would have to be increased to minimize shot noise) and the drift length of electrons (allowing thicker devices, lower capacitance, and thus lower series noise).

Uniformity requirements of detectors

In the discussion up until this point we have assumed that the material from which we construct our orthogonal strip detector is perfectly homogenous; that the resistivity, mobility and trapping lifetime are the same everywhere in the detector. However, as we will see in a later section of this paper, large variations in these properties commonly occur in presently available CZT crystals. Predicting the effect of material non-uniformities, of course, depends on the particular distribution in the sample in question, but a few general statements can be made. The noise will, in general, be affected most by the average local resistivity which will cause local fluctuations in the current density and hence the shot noise. An extreme example (but not uncommon in existing CZT) is the presence of a very localized conductive region in an otherwise high resistivity sample. The small conducting region would make a strip inoperable because of the large amount of shot noise it would generate, despite the fact that it occupies only a very small fraction of the strip area. We do not expect significant fluctuations in the dielectric constant throughout the sample; therefore, the series noise will be unaffected by material irregularities.

Another more subtle effect of electrical property fluctuations throughout the sample, and an effect particular to imaging detectors, is the change in the active volume of a given pixel (or strip) depending on the local values of the electrical characteristics under each particular strip. Of course, it is very undesirable in an imaging system to have different collection volumes for each strip because it results in a image with different effective pixel sizes. There are at least two electrical parameters that we have measured which exhibit substantial spatial variation through typical CZT samples: the resistivity and the mobility trapping time product ($\mu\tau_e$). In the following section we consider what effect these variations might have on the active volume of a pixel in an orthogonal strip detector.

The active volume of a given strip may be thought of as the volume defined by all electron trajectories that take a given time to reach that particular strip. For the case of a spectrometer, this trajectory time might be about one tenth of the electron trapping time and, in the case of a counter, this time might be the integration time of the shaping amplifier (determined by signal to noise considerations).

To illustrate the effects material variations may have on collection volumes, we used an approximate solution to Laplace's equation derived by He⁷ with boundary values similar to those encountered in a typical orthogonal strip detector. This potential distribution is shown in Figure 4.

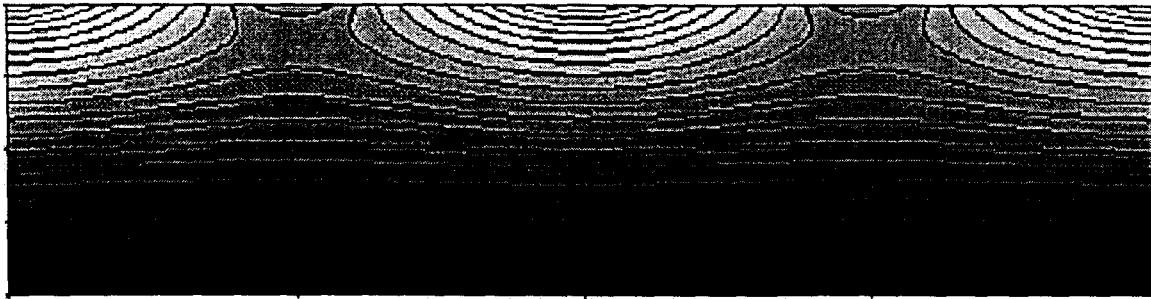


Figure 4.. Contour plot of the potential distribution in a strip detector obtained using the solution to Laplace's equation suggested by He⁷. The boundary values used to generate the solution were: strip pitch = 1.0 mm, detector thickness = 2.0 mm, strip width = 40 μm . A 4.0 mm wide cross-section of the hypothetical device is shown. For clarity of illustration, one strip was set to a potential of 200 V, and the adjacent strip to a potential of 100V.

We consider the case of a hypothetical strip detector which relies only on the collection of electrons at the positively biased strip. Next, we compute the electric field in the detector, and compute the trajectories of electrons that terminate on the strip. We can define the collection volume of a particular strip as the volume enclosed by electron trajectories that terminate at the periphery of the strip. Using this computation model we can compute the collection volume of a strip detector under conditions where the substrate has non-uniform electrical characteristics.

First, we consider the case of an orthogonal strip detector fabricated on a CZT substrate where the resistivity is different under different strips. Referring to Figure 5, if the resistivity under strip #1 is lower than the resistivity under strip #2 more current will flow through strip #1 and, because of the necessity of a large value resistor on the HV power supply line, the potential at strip #1 will be lower than the potential at strip #2. Of course, the value of the resistor in the HV power supply line will affect the voltage drop across it. For optimal signal to noise considerations the value of the bias resistor, R , should be as high as possible, but a realistic trade-off between the signal to noise ratio and dropping bias on the resistor is to set R to be about 10% of the strip resistance¹². Thus, if the resistivity of the substrate is locally changed by a factor of two we would expect about a 10% difference in the potential between the strips. As an example, consider a typical CZT strip detector constructed on a 2.0 mm thick substrate with a strip pitch of 1 mm with 20 % of the surface metallized with one strip at a potential of 200V while another strip is at a potential of 180 V. By computing the volume bounded by electron trajectories at the contact periphery, we compute that the active volume of the 200 V strip is 25% larger than the active volume of the strip at 190 V.

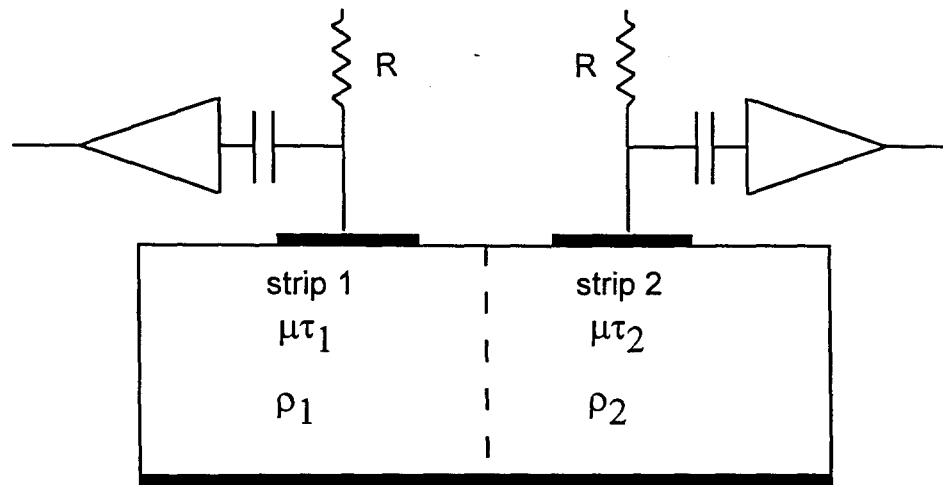


Figure 5.. Diagram of hypothetical distribution in electrical properties used to compute the effect of material inhomogeneities on strip detector performance.

Next we consider the hypothetical case where we hold the resistivity of the substrate constant (same potential on all strips) but we vary the electron lifetime in the region under one strip compared with another strip. We calculate the trajectories the same way as in the previous example, but truncate the trajectories when their arrival time is greater than 300 ns from the contact. This corresponds to the condition (discussed earlier) that the charge collection is equal to 90% at the terminus of the trajectory. Performing this type of calculation for a factor of two change in the local lifetime (from 3 μ s to 1.5 μ s with a constant mobility of 1000 $\text{cm}^2\text{V}^{-1}\text{s}^{-1}$) and using the following boundary conditions: 2.0 mm thick CZT with a strip pitch of 1.0 mm with 50 % of the surface metallized with both strips at a potential of 100V. Under these conditions we estimate the collection volume of the strip on 3 μ s material to have a collection volume two times larger than the strip located over the 1.5 μ s lifetime material. Note however, that these fluctuations in collection volume can be minimized by using a thin detector where the thickness of the detector is much less than the drift length of the carriers under constant field conditions. Further reductions in strip collection volume fluctuation could be obtained by making the fraction of metallization as high as possible.

These calculations indicate that fluctuations in the electrical properties of CZT substrates would lead to significant variations in the active detection volume of a strip.

Measured properties of existing CZT

Having discussed the implications of material properties on strip detector properties and design, it is useful to examine the properties of real CZT crystals that are currently available. We have performed extensive characterization on large quantities of CZT material in our laboratory as part of an effort to improve the quality of such material, and have an extensive data base of the electrical and optical properties of these crystals. We review briefly some recent data we have obtained on CZT samples to provide a perspective on what material is actually available today for use in orthogonal strip detectors

Perhaps the most obvious measure of uniformity in a CZT boule is its crystallinity. Unlike silicon or gallium arsenide where large single crystal boules are routinely grown, CZT boules produced today are polycrystalline. Although it is possible to make a detector from a sample of a CZT crystal containing more than one crystal grain, our studies indicate that such a sample would probably not be acceptable for fabricating an orthogonal strip detector. **Figure 6** and **Figure 7** show some typical distributions of grain sizes in slices of CZT boules we have measured in our laboratory. From these data, we can see that the yield of square single crystals with area larger than about 2 cm^2 is small. Thus it would be very expensive - at the current state of CZT crystal growth technology- to obtain samples of 10 cm^2 area (for instance) to use in orthogonal strip detectors, because of manufacturing yield considerations. At the present level of CZT manufacturing technology, a designer of instruments utilizing strip detectors would be wise to restrict her or his design to elements of no larger than about 2 cm^2 , or risk excessive cost and delay in building an instrument.

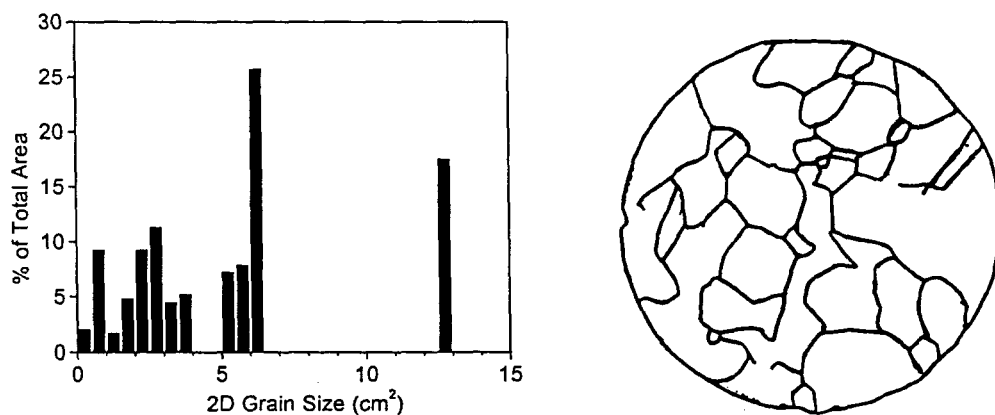


Figure 6. Distribution and the areal contribution (as a percent of the total area) of the various grain sizes in a 73 cm^2 CdZnTe wafer

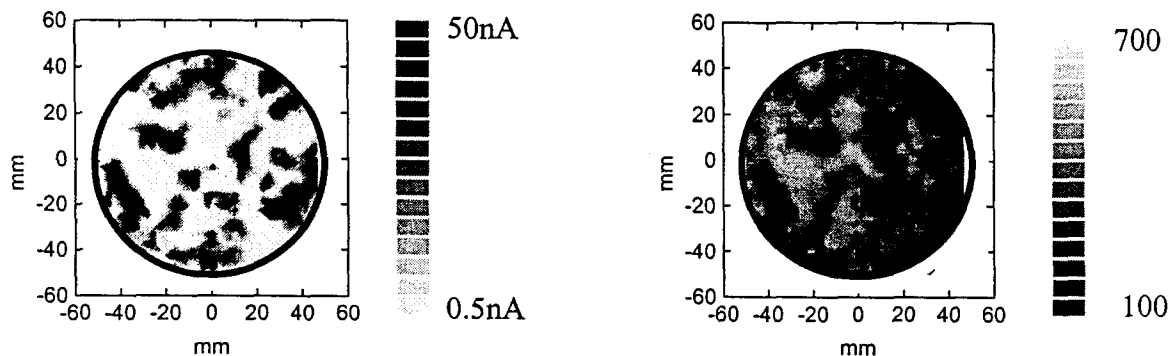


Figure 7. (a) Variations of the leakage current (in nA) throughout a CdZnTe wafer . If we assume that the contacts were Ohmic, these data indicate the distribution in the resistivity of the sample (b) Variations of the maximum alpha particle pulse height (in peak channel position), which gives an indication of the distribution of the electron drift length in this CdZnTe wafer.

Even within a single crystal grain there are many types of imperfections that may reduce the yield of useful strip detectors. For instance, **Figure 8** shows a type of localized defect that is fatal to device operation. Fortunately these local defects can be found fairly easily by visual inspection through an infra-red (IR) microscope, and it is feasible to avoid these regions before a sample is selected for strip detector manufacture.

In addition to the visually apparent irregularities discussed above, we have found that the measured electrical properties in samples of CZT also vary considerably across sections of a CZT boule. Some measurements obtained on apparatus designed specifically for this purpose are shown in **Figure 9**. Note that the variation in electrical properties shown in **Figure 9** exceed the range of variation used for the calculations performed in the previous section of this paper. Thus, we might expect significant fluctuations in the active volume of pixels in an orthogonal strip detector built on existing commercial CZT material

Summary

In this paper we reviewed the material requirements necessary to fabricate orthogonal strip detectors; focusing our attention on CZT. We found that limitations on the geometry of strip detectors are imposed by the electrical properties of the CZT crystals used to make such devices. We also determined that the thickness of a strip detector operated as a spectrometer is limited by the mobility lifetime product of existing material to a thickness of no greater than about 5 mm. Examination of the effect that the resistivity and thickness had on the noise produced in orthogonal strip detectors indicated that noise constraints are not a major issue in detector fabricated from CZT available today. We found that additional constraints on the maximum size, yield and expense of orthogonal strip detectors are imposed by the irregularities and non-uniformities present in available CZT samples. Thus, the mean properties of existing CZT material should be acceptable to build even very large area orthogonal strip detectors with good performance (provided they are no thicker than about 5 mm). However, fluctuations in the physical and electrical characteristics of existing CZT crystals significantly reduce the yield of devices. Furthermore, the imaging performance of detectors made from existing CZT crystals may be degraded from fluctuations in the electrical properties in the crystal used to fabricate the detector.

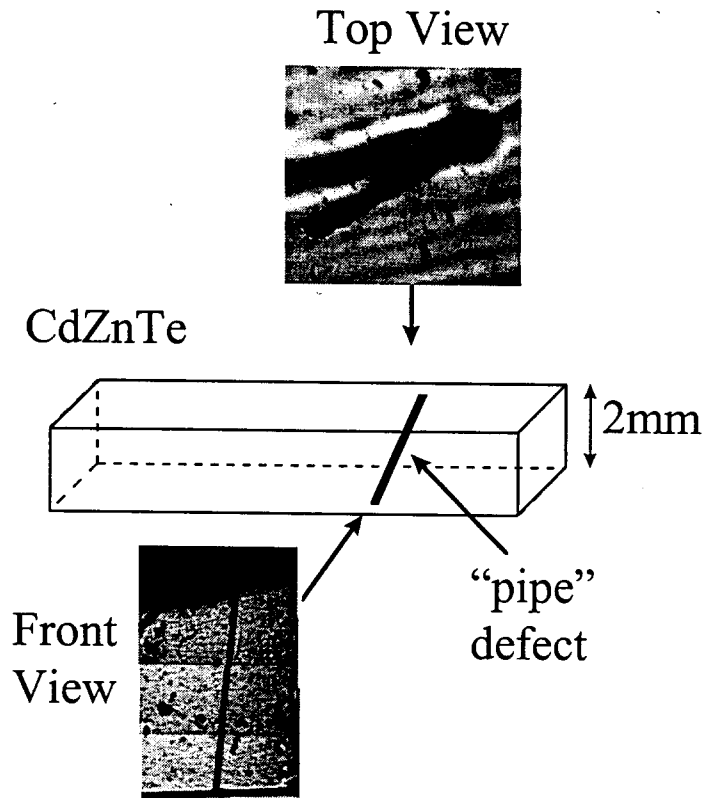


Figure 8. Schematic drawing of a CdZnTe sample containing a “pipe” defect and its top and front IR photographs. This “hollow tube” can be detrimental to the detector by providing a conductive path between the metal contacts, with the potential of shorting out the device. Indeed, this particular sample did result in a shorted device when tested under this configuration..

Acknowledgments

We gratefully acknowledge support of this project by Sandia National Laboratories Laboratory Directed Research and Development (LDRD) funds (#3514.090).

References

1. M.S. Gerber, D.W. Miller, P.A. Schlosser, J.W. Steidley, and A.H. Deutchman, *IEEE Trans. Nuc. Sci*, NS-24, p. 182, (1977).
2. Zanio, **Semiconductors and Semimetals**, Vol. 13, Academic Press, New York, 1978, p. 76.
3. S.M. Sze, **Physics of Semiconductor Devices**, John Wiley and Sons, New York, 1981, p.850.
4. P.N. Luke, *Applied Physics Letters*, **65**, (22) p.2884-2886 (1994).
5. P.N. Luke, *IEEE Transactions on Nuclear Science*, **42**, (4) p. 207-213 (1995)
6. V. Radeka, *Ann. Rev. Nucl. Part. Sci.*, **38**, p. 217, (1988).
7. Z. He, *Nucl. Inst. and Meth.*, **A365**, p. 572, (1995)
8. J.A. Henué, J.K. Brown, and B.H. Hasegawa, *Two-Dimensional Modeling of Compound-Semiconductor Strip Detectors*, presented at IEEE Nuclear Science Symposium, Anaheim, CA November, (1996)
9. E. Gatti, P.F. Manfredi, M Sampietro, and V. Speziali, *Nucl. Inst. And Meth.*, **A297**, p. 467, (1990).
10. G. Bertuccio, A. Pullia, and G. De Geronimo, *Nucl. Inst. and Meth.*, **A380**, p. 301, (1996)
11. F. M. Klassen, *IEEE Trans. Nuc. Sci*, **ED-18**, p. 97 (1971)
12. F. Olschner, Cremat, Inc., Watertown, MA, *Personal Communication*, (1997).

Orthogonal Strip Gamma Ray Imaging System for Use with HgI₂ and Cd_{1-x}Zn_xTe Detectors

N.R. Hilton¹, J.C. Lund², J. McKisson³, B.A. Brunett⁴, J.M. Van Scyoc⁵, R.B. James², and H.B. Barber¹

¹University of Arizona, Tucson AZ 85724

²Sandia National Laboratories, Livermore CA 94551

³RTI, Inc., Alachua, FL 32615

⁴Carnegie Mellon University, Pittsburgh, PA 15213

⁵University of California, Los Angeles, CA 90024

Abstract

We have designed and constructed an orthogonal strip imaging system for use with room temperature semiconductor strip detectors. The system has been tested with both HgI₂ and Cd_{1-x}Zn_xTe (CZT) detector elements. Our first system consists of complete readout electronics and software for spectroscopy and imaging with 8x8 orthogonal strip detectors. The readout electronics consist of 16 channels of hybrid charge sensitive preamplifiers, and 16 channels of parallel discriminators, shaping amplifiers, and a 16 channel ADC implemented in CAMAC and NIM. The software used to readout the instrument is capable of performing intensity measurements as well as spectroscopy on all 64 pixels of the device. In this paper we describe measurements to determine the factors limiting the performance of this system.

Keywords: Cadmium Zinc Telluride, Mercuric Iodide, Orthogonal Strip Detector, Gamma-Ray Imaging

1. Introduction

The application for which this gamma camera was developed is the monitoring of radioactive waste, stored nuclear materials, and medical applications (such as a miniature gamma camera for intraoperative use). However, the camera described in this paper does not have performance sufficient for these applications, instead our intention was to use this device as a platform to aid in the development of more sophisticated gamma cameras to be developed at Sandia National Laboratories.

2. Description of Instrument

Overview

The primary factor that determined the design of our gamma camera was the nature of the position sensitive radiation detector used as the basis of the system. We elected to use an orthogonal strip design as the position sensitive detector in our camera. The orthogonal strip design was first described by Gerber et al¹, and has received much recent attention for applications in astrophysics where high pixel counts are needed in coded aperture gamma-ray telescopes^{2,3,4}. The orthogonal strip design is attractive because it requires only 2 x N channels of electronics to readout an N² array of pixels; thus minimizing the cost and complexity of the read-out electronics. Of course, for high count rate applications with a large number of pixels, the orthogonal strip design starts to lose these advantages. In these cases, integrated circuits can readily provide the needed channel density for the readout of a pixellated detector without limiting the count rate to one event per read cycle⁴.

The system we constructed was designed such that detectors could be readily inserted into the front-end read-out electronics as a distinct mechanical module using a standard electronic package (24 pin dual in-line package), as opposed to wire bonding the detector directly to the input of the preamplifiers. The disadvantage of this modular approach is that additional noise may be added by the interconnections and longer circuit foil traces between detector and preamplifier. The primary advantage of this design is that it allows a variety of detectors to be tested relatively easily without re-fabricating the front-end of the instrument each time a detector is changed. Thus, this instrument is particularly useful for testing various detector designs. The details of the design and construction of the hardware and software that comprise this instrument are described in another paper⁶. In this paper we wish to focus on the performance characteristics of this instrument; nonetheless, a brief review of the hardware and software that comprise this instrument is given here so that the measurements performed with this instrument can be more clearly understood.

The detectors were 8x8 orthogonal strip devices fabricated on HgI₂ and CZT substrates approximately 2.0 mm thick design with an active area of approximately 1cm². These devices were placed on chip carriers that allowed them to be plugged directly into the readout electronics. Detectors were fabricated by evaporating metal contacts on to the surface of etched

crystal substrates using a shadow mask to define the strip pattern. A total of four detectors were fabricated: three from CZT and one from HgI₂. The detectors were mounted on standard 24 pin alumina dual in-line packages (DIPs) commonly used for hybrid electronic circuits. Fine gold wires (25 μm diameter) were bonded to the metal contact strips using silver epoxy, the other end of the wire was then bonded to a metal foil pattern on the alumina substrate of the dual inline package. The packaged detectors could then be inserted directly into a socket on the front-end readout circuit board.

The electronic system used to readout the detectors consisted of 8 channel hybrid preamplifiers (Lecroy HQV 820), system-by NIM and CAMAC readout amplifiers and ADCs. The performance of the readout system is determined largely by the hybrid preamplifiers which first amplify the signals from the 8x8 detector array; the rated performance of the preamplifiers translates to about 5 keV FWHM of noise referenced to a CZT gamma spectrum.

Software was written to readout the coincident signal from the strip detector, decode the pixel position, and visualize the gamma ray intensity distribution at the detector plane. The software interrogated the ADCs and discriminators in the CAMAC crate, decoded the position of interaction on the orthogonal strip detector, and created pulse height spectra of the interactions that occurred at each pixel. Another function of the software was to provide real time feedback on the operation of the camera, and diagnostics of various camera functions (such as cross-talk between channels). The software was written in the high level control language "Kmax" to minimize development and reduce the amount of time spent writing low level CAMAC control routines.

3. Performance of Camera

After we had assembled and debugged the camera hardware and software, we began testing the ability of the camera to measure the energy distribution of isotopic sources using pulse height spectroscopy and to form an image of a radioactive source using a pin-hole collimator to project the image onto the detector plane.

Image Formation

A pin-hole collimator was placed between gamma-ray photon sources and the detector and images acquired with the system. Such an image is shown in Figure 1. The ability to discriminate sources of a particular energy was verified and some results are also shown in Figure 1.

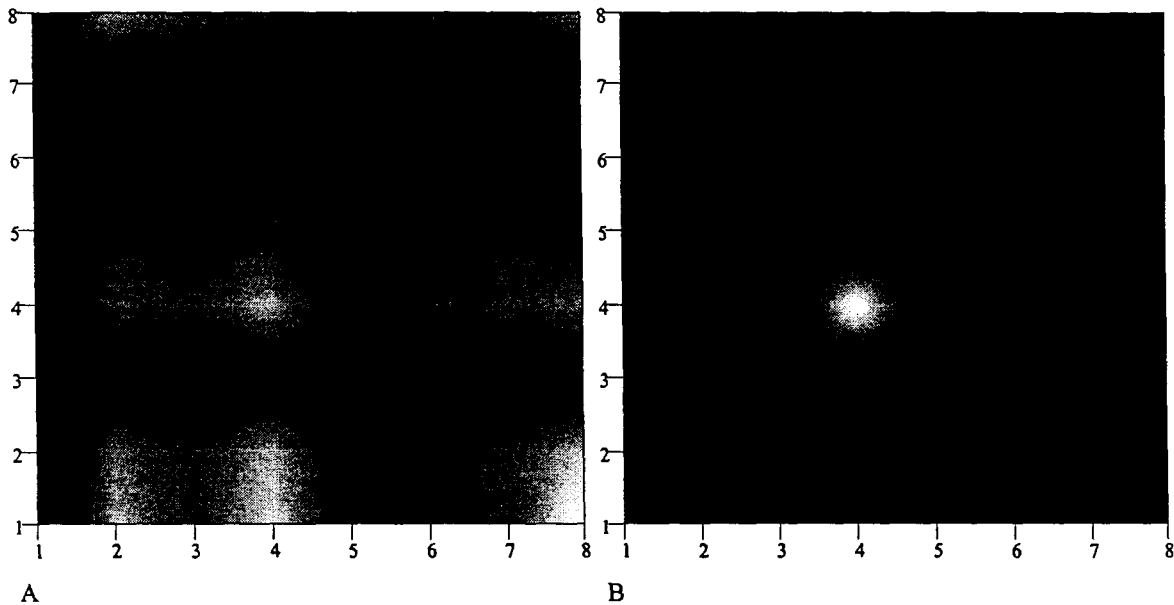


Figure 1. Pinhole images of a ¹³³Ba point source while the detector was flood illuminated by an ²⁴¹Am source from behind. B is the same as A except with an energy window of greater than 70 keV applied.

Signal Propagation

Additional measurements were performed with the camera system to determine if the signals produced by the detector matched our expectations based on the design of the detector elements and readout electronics. Figure 2 show some typical waveforms from adjacent strips observed at the output of the analog signal processing chain (preamplifier and shaping amplifier) with a digital oscilloscope. This cursory examination of the signals with an oscilloscope indicated that electronic “cross-talk” was not a significant problem. A more careful study of charge sharing between adjacent strips was performed with the apparatus shown in Figure 3. Some results obtained with this apparatus are shown in Figure 4; analysis of these data indicated that the ratio of events shared between strips (with flood-field irradiation of the strip detector) is consistent with what would be expected based on the fraction of metallization on the surface of the strip detector.

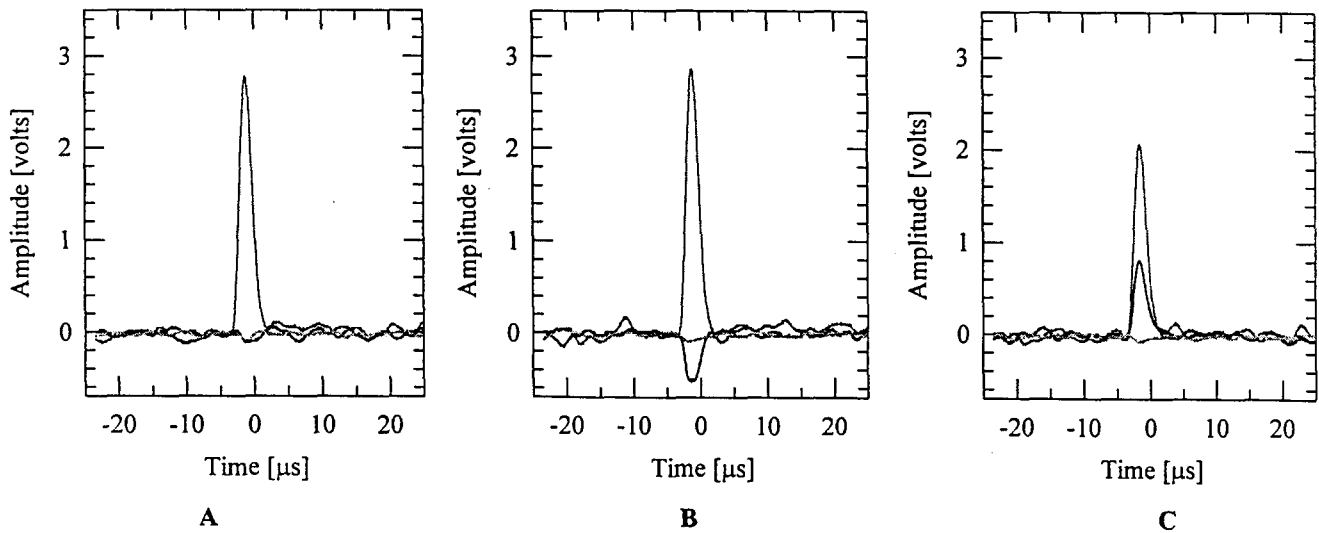


Figure 2. Waveforms observed with a digital oscilloscope when observing the output of the shaping amplifiers from three adjacent strips on an 2 mm thick 8x8 CZT detector with a strip pitch of 1.0 mm. The detector was being irradiated with a ^{133}Ba source. Plot A is the most common waveform observed at the output; all of the signal appears localized to one strip. The output in Plot B is observed much less commonly and may arise from an event generating electrons on the opposite of the detector and drifting toward the strips being observed. Initially, the same polarity current would be induced on both strips, but when the electrons near one strip, we would expect a current of opposite polarity to be generated on the adjacent strip. Plot C is a waveform that probably corresponds to an event occurring somewhere between two adjacent strips with current being induced on both strips.

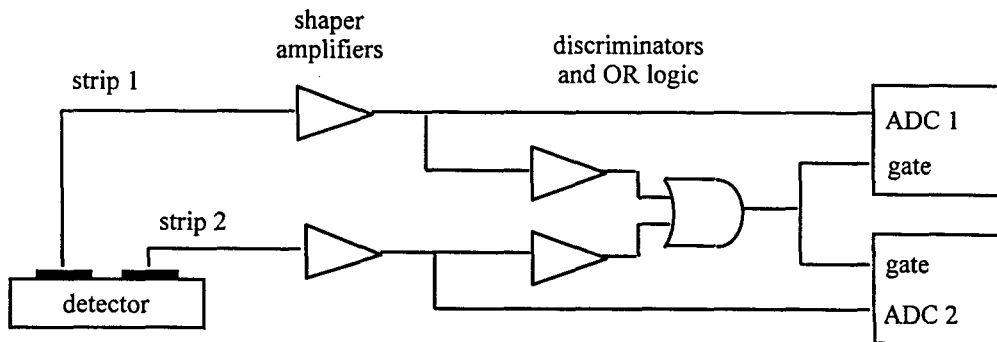


Figure 3. Apparatus used to measure the simultaneous pulse height spectra from two adjacent strips. The ADCs used to measure pulse heights were triggered on a signal from either of the two strips.

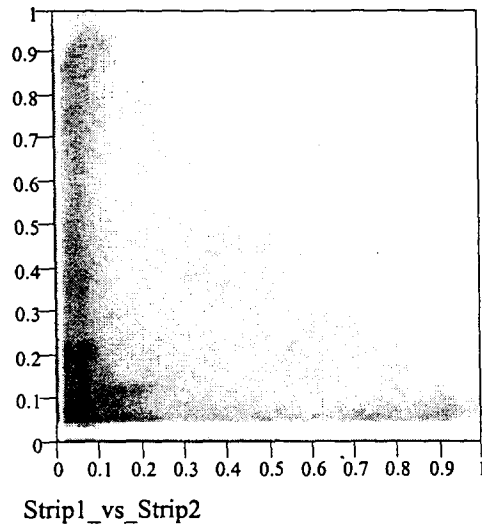


Figure 4. Contour plot of pulse height spectra acquired simultaneously on two adjacent strips of a CZT strip detector irradiated with photons from a ^{133}Ba source. The ADCs used to measure pulse heights were triggered on a signal from either of the two strips.

Energy Resolution

The applications we are interested in require the gamma camera to simultaneously estimate the position of gamma ray emissions as well as measure the energy distribution of the sources; thus the energy resolution of the detector system is of great interest. A typical pulse height spectrum obtained from a single strip of one of our CZT strip detectors is shown in Figure 5. Examination of Figure 5 reveals that two factors degrade the pulse height resolution in the strip detectors: Gaussian broadening due to electronic noise and - for higher energy photons- an asymmetric distortion of the peaks due to incomplete charge collection effects. We have measured the contribution of both noise and charge collection broadening and report on it below.

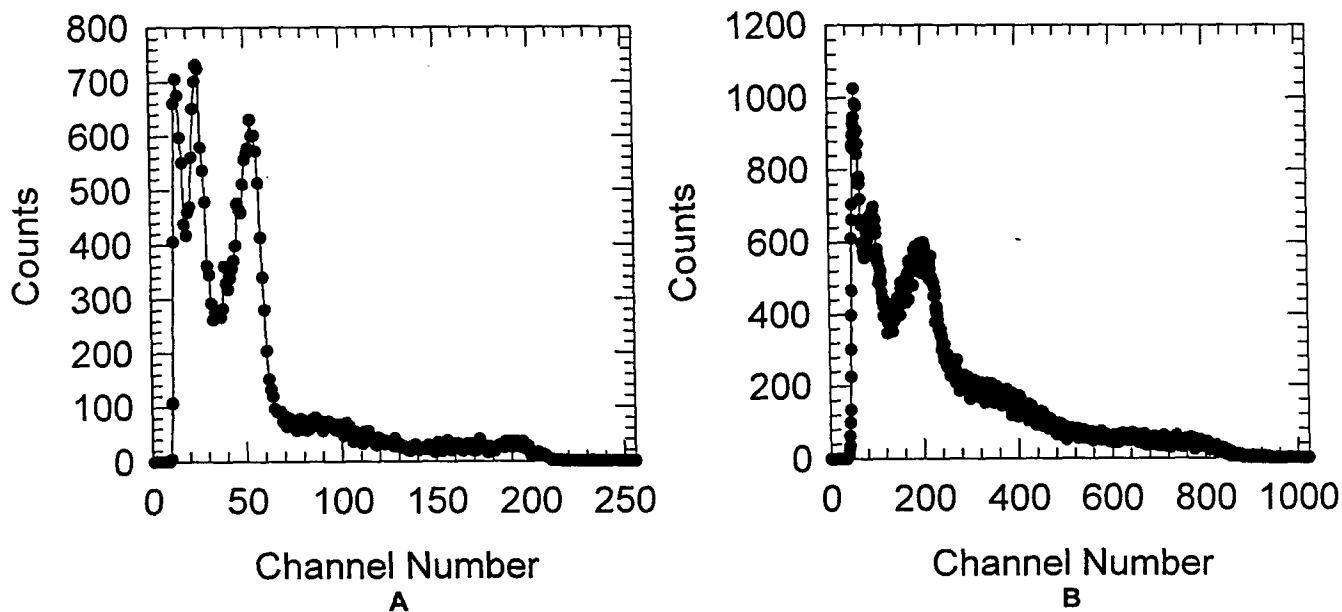


Figure 5. Pulse height spectra obtained by irradiating an 8x8 CZT orthogonal strip detector with photons from a ^{133}Ba source. Plot A shows a typical pulse height spectrum obtained by interrogating one strip in the detector. The pulse height spectrum shown in Plot B was obtained by summing the pulse height spectra from all eight rows in the detector. Some degradation in energy resolution occurs when multiple rows (or columns) are summed because: 1. the noise broadening is

determined by the noisiest strip, and 2. the system software does not always correct perfectly for the fluctuations in the gain of each readout channel.

Electronic Noise Contribution

The relative contribution of the electronic noise to the pulse height spectrum broadening was measured by injecting a fixed amplitude charge pulse to the input of the preamplifier and measuring the width of the peak produced by the charge pulses in the pulse height spectrum under various conditions. Figure 6. shows a plot of the measured electronic noise as a function of linear amplifier time constant (semi-Gaussian shaping). Because there was no convenient way to inject charge pulse of known absolute amplitude into the front end of the preamplifier, a CZT pulse height spectrum of ^{241}Am (59.5 keV peak) was used to calibrate the charge gain of the system. A value for the average charge pair creation energy in CZT of 5.0 eV was assumed in the calculations. Noise measurements were also performed on the same detector strip using different readout electronics and the results are also shown in Figure 6. Using the conventional methods for analyzing the properties of detector system noise sources⁷, the results in Figure 6 indicate that the dominant noise source in the detector system is a parallel source. The fact that the parallel noise source is present even when there is no bias applied to the detector, indicates that the parallel noise source is not due to leakage current in the detector (shot noise), more likely, the parallel noise contribution is from the resistive feedback in the charge amplifier array.

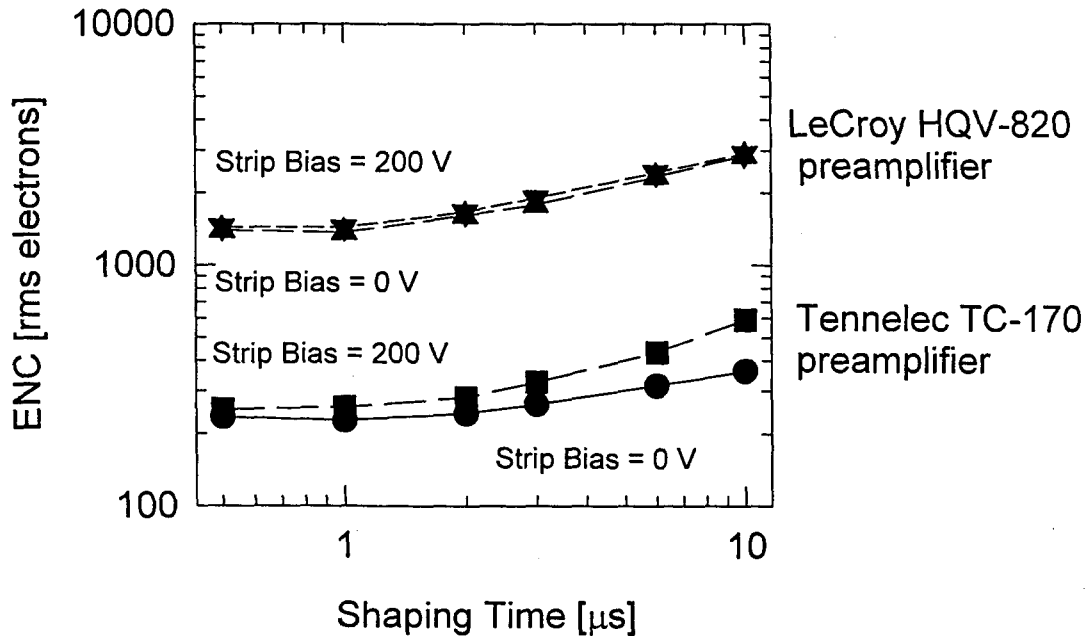


Figure 6. Equivalent noise charge (ENC) versus amplifier shaping time (semi-Gaussian shaping) for a single strip of a CZT 8x8 orthogonal strip detector. Two different sets of readout electronics were used: 1. a single channel of the LeCroy 8 channel hybrid preamplifier used in our imaging camera prototype, and 2. a standard single channel charge sensitive preamplifier (Tennelec TC-170). The single channel preamplifier contributed much less noise than the 8 channel unit used in our camera. The general increase in the noise magnitude with increasing shaping time indicates that the noise broadening in the pulse height spectrum was dominated by 1/f and parallel white components. With the LeCroy preamplifier the parallel noise source was probably the feedback resistor in the charge sensitive preamplifier, as shot noise had no measurable contribution to the noise (no difference was measured in the noise with the bias on and off in the detector). Note that 1000 electrons rms of ENC corresponds to approximately 12 keV FWHM in the pulse height spectrum of a CZT detector.

Charge Collection Broadening

When the ratio of the strip pitch to the detector thickness is greater than one, we leave the “small pixel” regime⁸ (both the electron and hole motion contribute to the induced charge on each contact strip). Under these conditions, an orthogonal strip detector behaves much like a conventional large area parallel contact detector. A common characteristic of pulse height spectra produced by conventional detectors made from room-temperature semiconductor detectors is the presence of “hole

tailing" in the gamma-ray photo-peaks. This asymmetrical broadening of the peaks toward lower pulse heights has been studied extensively^{9,10} and arises from the short drift length of holes relative to the detector thickness. Because the holes drift only a fraction of the distance between the contacts, the charge collected on the contact depends on the depth of interaction of the gamma-ray photon in the crystal. The shapes of the peaks in the pulse height spectra that we observed were dominated by hole tailing effects at energies greater than about 100 keV; consistent with the penetration distances of photons in CZT, and the poor hole drift length in this material. These effect can be seen in the pulse height spectra shown in Figure 5.

4. Summary

We have designed, built and tested a small gamma camera based on an orthogonal strip detector design. The gamma camera utilizes "8x8" strip detectors made from either CZT or HgI₂. The camera is able to measure the position of interaction of single gamma ray photons (of energy greater than ~ 10 keV) on the detector plane and estimate the energy distribution of gamma-rays interacting with the detector using pulse height spectroscopy methods. We examined the factors that limit both the spatial resolution of this system and the energy resolution when operated as a pulse height spectrometer.

The position resolution of the detector was limited largely by the small number of pixels such that position resolution was only one in eight in each direction. The basic design and construction techniques used in the camera were measured to be sound however, as little or no cross-talk was observed between strips in the detector, and these same methods could be used to build devices with a higher density of strips and better relative position encoding.

The energy resolution of the system was also examined when operated as a pulse height spectrometer. It was found that the energy resolution was limited at lower photon energies (< 150 keV) by Gaussian broadening due to electronic noise, and at higher photon energies to charge collection effects. The electronic noise was dominated by the readout amplifiers and not controlled by leakage current in the detector. Thus, a significant improvement in the performance of the system could be realized (particularly at lower energies) through improvements in the electronic readout system.

Acknowledgements

All of the work described in this paper was performed at Sandia National Laboratories, Livermore CA, and we are grateful to the management at Sandia for allowing student participation in this project. We gratefully acknowledge financial support for this project from Laboratory Directed Research and Development (LDRD) funds (#3514.090 and #1135.100).

References

1. M.S. Gerber, D.W. Miller, P.A. Schlosser, J.W. Steidley, and A.H. Deutchman, *Position Sensitive Gamma Ray Detectors Using Resistive Charge Division Readout*, IEEE Trans. Nuc. Sci, NS-24, p. 182, (1977).
2. J.L. Matteson et al, *CdZnTe strip detectors for high-energy x-ray astronomy*, Proc. SPIE Vol. 2859, p. 58, (1996)
3. C.M. Stahle, et al, *CdZnTe strip detector for arcsecond imaging and spectroscopy*, Proc. SPIE Vol. 2859, p. 74, (1996)
4. J.R. Macri, et al, *Progress in the development of large-area submillimeter-resolution CdZnTe strip detectors*, Proc. SPIE Vol. 2859, p. 29, (1996).
5. H.B. Barber, *CdZnTe arrays for nuclear medicine imaging*, Proc. SPIE Vol. 2859, p. 26, (1996).
6. J.C. Lund et al, *Orthogonal Strip Gamma-Ray Imaging System for use with HgI₂ and CdZnTe Detectors*, Presented at the MARCIV conference Kona, HI April (1997).
7. V. Radeka, *Low-Noise Techniques in Detectors*, Ann. Rev. Nucl. Part. Sci., 38, p. 217, (1988).
8. J.D. Eskin, H.B. Barber, H.H. Barrett, *Variations in pulse-height spectrum and pulse timing in CdZnTe pixel array detectors*, Proc. SPIE Vol. 2859, p. 46-49, (1996)
9. R.O. Bell, *Calculation of Gamma-Ray Pulse Height Spectrum in a Semiconductor Detector in the Presence of Charge Carrier Trapping*, Nucl. Inst. and Meth., 93, p. A2, (1971).
10. W. Akutagawa and K. Zanio, *Gamma Response of Semi-Insulating Material in the Presence of Trapping and Detrapping*, J. Appl. Phys., 40, p. 3838, (1969).

DISTRIBUTION:

- 1 Richard Malenfant
U. S. Department of Energy
Office of Research and Development, NN-20
1000 Independence Avenue, S.W.
Washington, D.C. 20585
- 1 Karl Reinitz
U. S. Department of Energy
Office of Research and Development, NN-20
1000 Independence Avenue, S.W.
Washington, D.C. 20585
- 1 Cal Moss
Los Alamos National Laboratory
NIS-2, MS D436
Los Alamos, NM 87545
- 1 Bob Scarlett
Los Alamos National Laboratory
P. O. Box 1663, MS D460
Los Alamos, NM 87545
- 2 T. E. Schlesinger
Department of Electrical and Computer Engineering
Carnegie Mellon University
5000 Forbes Avenue
Pittsburgh, PA 15213
- 1 A. Burger
Department of Physics
Fisk University
Nashville, TN 37208
- 1 M. Roth
Graduate School of Applied Science
Hebrew University of Jerusalem
Givat Ram 9
Jerusalem, Israel 91904
- 1 M. Goorsky
Department of Materials Science and Engineering
University of California at Los Angeles
Los Angeles, CA 90095-1595
- 1 Hojun Yoon
Department of Materials Science and Engineering
University of California at Los Angeles
Los Angeles, CA 90095-1595

Distribution: (Continued)

- 1 Y. C. Chang
Department of Physics
University of Illinois
1110 West Green Street
Urbana, IL 61801

- 1 Glenn Knoll
Dean, College of Engineering
University of Michigan
2309 EECS Building
Ann Arbor, MI 48109-2116

- 1 W. Yao
Department of Electrical Engineering
University of Nebraska
P. O. Box 8806511
Lincoln, NB 68588

- 1 Jack Trombka
Senior Goddard Fellow
Goddard Space Flight Center
MC 691, Bldg. 2, Rm. 235
Greenbelt, MD 20771

- 1 Warnick Kernan
Remote Sensing Lab
4600 N. Hollywood Blvd., Bldg. 2211
Las Vegas, NV 89191

- 2 X. J. Bao
TN Technologies, Inc.
P. O. Box 800
Round Rock, TX 78680

- 1 J. Cook
TN Technologies, Inc.
P. O. Box 800
Round Rock, TX 78680

- 3 M. Natarajan
TN Technologies, Inc.
P. O. Box 800
Round Rock, TX 78680

- 1 MS0107 V. Portillo
- 1 MS0188 D. Chavez
- 1 MS0351 R. C. Hughes
- 1 MS0469 J. M. Taylor
- 1 MS0503 G. R. Laguna
- 1 MS0525 K. O. Wessendorf
- 1 MS0571 R. L. Ewing
- 1 MS0656 D. L. Mangan

Distribution: (Continued)

| | | |
|---|--------|--|
| 1 | MS0768 | R. Moya |
| 1 | MS1071 | M. R. Daily |
| 1 | MS1380 | D. Larson |
| 1 | MS1380 | D. Rix |
| 1 | MS1380 | R. Calvert |
| 1 | MS9004 | J. Vitko |
| 1 | MS9001 | T. O. Hunter |
| | | Attn: P. N. Smith, MS9002 |
| | | D. L. Crawford, MS9003 |
| | | M. E. John, MS9004 |
| | | J. B. Wright, MS9005 |
| | | R. C. Wayne, MS9007 |
| | | P. E. Brewer, MS9141 |
| | | W. J. McLean, MS9054 |
| 1 | MS9014 | W. G. Wilson |
| 1 | MS9141 | A. Freudendahl |
| 1 | MS9161 | A. Pontau |
| 1 | MS9161 | D. Cowgill |
| 1 | MS9161 | J. Markakis |
| 1 | MS9161 | J. VanScyoc |
| 2 | MS9161 | M. Schieber |
| 1 | MS9161 | R. J. Anderson |
| 1 | MS9162 | D. Morse |
| 1 | MS9162 | L. Franks |
| 1 | MS9402 | A. Antolak |
| 1 | MS9402 | D. Medlin |
| 1 | MS9403 | J. C. F. Wang |
| 1 | MS9404 | C. Perrino |
| 1 | MS9404 | G. Buffleben |
| 6 | MS9405 | J. C. Lund |
| 1 | MS9405 | J. M. Hruby |
| 1 | MS9405 | R. B. James |
| 1 | MS9409 | R. Stulen |
| 1 | MS9420 | L. A. West |
| | | Attn: L. N. Tallerico, MS9430 |
| | | C. W. Sumpter, MS9912 |
| | | B. E. Affeldt, MS9133 |
| | | M. H. Rogers, MS9420 |
| | | A. J. West, MS9430 |
| 1 | MS9671 | E. Cross |
| 1 | MS9671 | H. Hermon |
| 1 | MS9671 | R. W. Olsen |
| 3 | MS9018 | Central Technical Files, 8940-2 |
| 4 | MS0899 | Technical Library, 4414 |
| 1 | MS9021 | Technical Communications Department, 8815/Technical Library, MS0899, 4414 |
| 2 | MS9021 | Technical Communications Department, 8815, for DOE/OSTI |